Adaptive Human Force Scaling for Physical Human-Robot Interaction via Admittance Control

by

Yahya Mohey Hamad Al-Qaysi

A Dissertation Submitted to the
Graduate School of Sciences and Engineering
in Partial Fulfillment of the Requirements for
the Degree of

Doctor of Philosophy

in

Mechanical Engineering

KOÇ UNIVERSITY

April 26, 2023

Adaptive Human Force Scaling for Physical Human-Robot Interaction via Admittance Control

Koç University

Graduate School of Sciences and Engineering

This is to certify that I have examined this copy of a doctoral dissertation by

Yahya Mohey Hamad Al-Qaysi

and have found that it is complete and satisfactory in all respects,

and that any and all revisions required by the final

examining committee have been made.

Committee Members:

____

Prof. Dr. Çağatay Başdoğan (Advisor)

____

Asst. Prof. Dr. Yusuf Aydın (Co-advisor)

____

Prof. Dr. Murat Sözer

____

Prof. Dr. Volkan Patoğlu

____

Assoc. Prof. Dr. Tufan Kumbasar

____

Assoc. Prof. Dr. Evren Samur

Date: ____________________________________

To my beloved family

ABSTRACT

Collaborative robotic systems are designed to be lightweight, portable and are equipped with inherent safety features. These qualities allow such robots to be situated in close proximity to humans, and even enable daily activities that require direct physical interaction with humans, such as object co-manipulation. Co-manipulation is prevalent in many industries, such as production, manufacturing, and construction, which still rely on manual labour of skilled manpower. Manipulating bulky and/or heavy objects are ergonomically hard, hence are typically handled by two humans in those industries, even though they are non-value-added tasks. Therefore, a collaborative robot can be introduced to assist the human partner in such manipulation tasks in order to decrease the human effort and save labor time. Nevertheless, if the robot is programmed to passively follow human movements, it would be an extra burden to the human partner, particularly when human movement intentions change during the task. On the other hand, if the robot executes the task based on pre-programmed plans without paying attention to the human partner's intentions, conflicts will arise, and if these conflicts are not resolved, the task will be exhausting for the human. Hence, for the robot to perform a collaborative manipulation task naturally and effectively, it has to be aware of human intentions and act accordingly.

In the first part of this dissertation, we design an admittance controller for a robot to adaptively change its contribution to a collaborative manipulation task executed with a human partner to improve the task performance. This has been achieved by adaptive scaling of human force based on her/his movement intention while paying attention to the requirements of different task phases. In our approach, movement intentions of human are estimated from measured human force and velocity of manipulated object and converted to a quantitative value using a fuzzy logic scheme. This value is then utilized as a variable gain in an admittance controller to adaptively adjust the contribution of robot to the task without changing the admittance time constant. We demonstrate the benefits of the proposed approach by a pHRI experiment utilizing Fitts' reaching movement task. The results of the experiment show that there is a) an optimum admittance time constant maximizing the human force amplification and b) a desirable admittance gain profile which leads to a more effective co-manipulation in terms of overall task performance.

In the second part of this dissertation, we propose a machine learning (ML) approach to resolve conflicts that may occur between human and a proactive robot during the

execution of a collaborative task. We suggest focusing on the dyadic interaction patterns to detect and resolve such conflicts. We further argue that the features derived from haptic (force/torque) data only as inputs to a ML algorithm is sufficient to classify if human and robot manipulate the object harmoniously or they face a conflict. In our approach, the robot contributes to the task proactively when there is harmony or follows human behavior passively when there is a conflict. We implement an admittance controller to regulate the physical interaction between human and robot during the task (hence, the robot follows the human passively when there is a conflict) and utilize an artificial potential field approach to make the robot proactive when the partners work in harmony. We designed experimental scenarios involving harmonious and conflicting interactions between human and robot during a collaborative manipulation of an object to train and test our ML model. The results of the study show that ML successfully detects the conflicts and reduces the human force and effort significantly compared to the case of a passive robot that always follows human partner and a proactive robot that cannot resolve conflicts.

In summary, in this dissertation, we propose pHRI approaches to adjust the contribution of the robot collaboratively manipulates an object with a human partner. Both approaches rely on the haptic data as inputs to the admittance controller to regulate the physical interaction between human and robot in an object co-manipulation task. Moreover, these approaches involve human intentions in their structures. In particular, in the first one, we introduce a rule-based estimation of human movement intentions and adapt the contribution of the robot to the manipulation task accordingly. On the other hand, in the second approach, since we consider a more complex scenario that involves a proactive robot, we take into account the dyadic intentions of both human and a robot in terms of the interaction behaviors that emerge between the partners during the co-manipulation task. We build a ML classifier that detects these behaviors and notifies the controller to adjust the role of the robot accordingly.

ÖZETÇE

Modern işbirlikçi robotik sistemler, hafif, taşınabilir olacak şekilde tasarlanmıştır ve düşük çalışma hızı gibi doğal güvenlik özellikleriyle donatılmıştır. Bu nitelikler, bu tür robotların insanlara yakın konumlandırılmasına ve hatta insanlarla doğrudan fiziksel etkileşim gerektiren günlük faaliyetlere olanak tanır. Buna rağmen, üretim, imalat ve inşaat gibi birçok endüstride hala insan gücüne dayalı ortak manipülasyon yaygındır. Örneğin, hacimli veya ağır objelerin taşınması ergonomik olarak zordur, bu nedenle, katma değeri olmasa bile tipik olarak iki kişi tarafından yapılır. Ortak bir obje manipülasyonunda, insanın harcadığı eforu azaltmak için işbirlikçi bir robot kullanılabilir. Bununla birlikte, bu robot insan hareketlerini pasif olarak takip edecek şekilde kontrol edilirse, özellikle görevi yerine getirirken insan hareket niyetleri değiştiğinde, onun için ekstra bir yük haline dönüşebilir. Öte yandan, robot insan partnerin niyetini dikkate almadan önceden programlanmış planlara göre görevi yerine getirirse, çatışmalar (anlaşmazlıklar) ortaya çıkacak ve bu çatışmalar çözülmezse, görev insan için yorucu olacaktır. Dolayısıyla robotun görevi doğal ve etkili bir şekilde yerine getirebilmesi için insanın niyetini bilmesi ve buna göre hareket etmesi gerekir.

Bu tezin ilk bölümünde, görev performansını iyileştirmek için bir insanla yürütülen işbirlikçi bir manipülasyon görevine katkısını uyarlamalı olarak değiştirebilen bir robot için bir admitans denetleyicisi tasarladık. Bu, görevin farklı aşamalarını dikkate alarak robotun göreve katkısını uyarlamalı değiştirerek başarılmıştır. Yaklaşımımızda, insanın hareket niyetleri, ölçülen insan kuvveti ve manipüle edilen nesnenin hızından tahmin edilir ve bir bulanık mantık şeması kullanılarak nicel bir değere dönüştürülür. Bu değer daha sonra zaman sabitini değiştirmeden robotun göreve katkısını uyarlamalı olarak ayarlamak için bir admitans denetleyicisinde değişken bir kazanç olarak kullanılır. Bu çalışmada, önerilen yaklaşımın faydalarını, Fitts'in hareket kuralını kullanan bir pHRI deneyi ile gösteriyoruz. Deneyin sonuçları, a) robotun katkısını en üst düzeye çıkaran optimum bir zaman süresi sabiti ve b) genel görev performansı açısından daha etkili ortak manipülasyonu sağlayan bir kabul kazanç profili olduğunu göstermektedir.

Bu tezin ikinci bölümünde, işbirlikçi bir görevin yürütülmesi sırasında insan ile proaktif bir robot arasında meydana gelebilecek çatışmaları çözmek için bir makine

öğrenimi (ML) yaklaşımı öneriyoruz. Bu tür çatışmaları tespit etmek ve çözmek için ortaklar arasındaki kuvvet etkileşimlerine odaklanmanızı öneriyoruz. Sadece dokunsal (kuvvet/tork) verilerden türetilen özelikleri girdi olarak alan bir makina öğrenmesi modelirin, insan ve robotun nesneyi uyumlu bir şekilde manipüle edip etmediğini veya bir çatışmayla karşılaşıp karşılaşmadıklarını sınıflandırmak için yeterli olduğunu savunuyoruz. Bizim yaklaşımımızda robot, uyum olduğunda göreve proaktif olarak katkıda bulunur veya bir çatışma olduğunda pasif olarak insan davranışını takip eder. Görev sırasında insan ve robot arasındaki fiziksel etkileşimi düzenlemek için yine bir admitans denetleyicisi kullanıyoruz. Makine öğrenmesi modelimizi eğitmek ve test etmek için bir nesnenin işbirlikçi manipülasyonu sırasında insan ve robot arasındaki uyumlu ve çelişkili etkileşimleri içeren deneysel senaryolar tasarladık. Çalışmanın sonuçları, makine öğrenmesinin çatışmaları başarılı bir şekilde tespit ettiğini ve insan gücünü ve çabasını, her zaman insan ortağını takip eden pasif bir robot ve çatışmaları çözemeyen proaktif bir robot durumuna kıyasla önemli ölçüde azalttığını göstermektedir.

ACKNOWLEDGEMENTS

First and foremost, I would like to thank my research advisor Prof. Dr. Çağatay Başdoğan for his support, patience, guidance, and valuable comments throughout my Ph.D. studies. Without his support, it would have been impossible for this dissertation to be accomplished.

I would also like to express my sincere gratitude to my research co-advisor Asst. Prof. Dr. Yusuf Aydın, whose contribution and support during my study had a great impact on the completion of this dissertation.

I would like to thank my Ph.D. thesis monitoring committee members Prof. Dr. Murat Sözer and Prof. Dr. Volkan Patoğlu for their time, interest, and comments during the progress of my thesis.

I would also like to express my deep and sincere gratitude to my family as a whole. Without their support and understanding, this work would not have been possible.

I would like to thank my dear friend Zaid Al-Saadi for supporting me and sharing with me all the good and hard times during my Ph.D. studies.

I would like to thank all former and current members of the Robotics and Mechatronics Laboratory (RML): Dr. Senem Ezgi Emgin, Dr. Yasemin Vardar, Dr. Ozan Çaldıran, Dr. Ömer Şirin, Dr. Khurram Saleem, Dr. Bushra Sadia, Milad Jamalzadeh, Utku Erdem, Aykut İşleyen, İdil Özdamar, Doganay Şirintuna, Mohammad Reza Chehrezad, Ceyhun Ibolar, Easa Aliabbasi, Pouya Pourakbarian Niaz, Aliriza Madani, Berke Ataseven, Volkan Aydınğül, Jahangier Ahmad, Muhammad Muzammil, Riaz Minhas. I am glad to know such kind and hardworking people.

I would also like to thank Sarah Hamdan, Berk Güler, and Feras Kiki for their special support and assistance during the last period of my research.

Finally, I would like to acknowledge and thank University of Baghdad for financially supporting me during my Ph.D. studies.

TABLE OF CONTENTS

LIST OF TABLES

LIST OF FIGURES

NOMENCLATURE

Acronyms

AI	artificial intelligence
ANN	artificial neural network
ANOVA	analysis of variance
APF	artificial potential field
CD	conflict in target direction
CP	conflict in parking location
EMG	electromyography
ES	experimental scenario
ID	index of difficulty
IP	index of performance
ML	machine learning
MT	movement time
pHRI	physical human-robot interaction
TCT	task completion time
WH	working in harmony

List of symbols

b_a	admittance damping
b_H	human arm endpoint damping
D	reaching distance
d_t	limit distance around the target
d_s	limit distance around the start point
F_R	force applied on an object by robot
F_{SUM}	summation forces applied by human and robot
F_H^*	effective force of human contribute to the task

F_R^*	effective force of robot contribute to the task
f_H	force applied by human
$F_H(s)$	laplace transformations of f_H
$\dot{f}_H$	derivative of human force
F_H^{ave}	average force applied by subject
F_R^{ave}	average force applied by robot to move the cart
F_{ATT}	attractive force
F_T	total force
F_H	force applied by human partner
G_H	scaling gain
$G(s)$	transfer function for robot
G_H^{nom}	nominal value of G_H
G_H^{max}	maximum allowable limit of G_H
G_H^{min}	maximum allowable limit of G_H
$H(s)$	low pass filter
I_H	weighting factor
K_a	admittance gain
K_{HII}	human Intention Index
$K_{\mathrm{HII}}^{\mathrm{m}}$	integrated human intention index
$\overline{K}_{\mathrm{HII}}^{\mathrm{m}}$	bounded value of $K_{\mathrm{HII}}^{\mathrm{m}}$
k_H	human arm endpoint stiffness
l	distance from start position to park position
m_a	admittance mass
m_H	human arm endpoint mass
$M_{E_K}^F$	individual force efficiencies
M_{TE}^F	team force efficiency
M_{NE}^F	negotiation force efficiency
M_S^F	similarity of forces
$M_{E_K}^T$	individual torque efficiencies
M_{TE}^T	team torque efficiency
M_{NE}^T	negotiation torque efficiency
M_S^T	similarity of torques
P^{ave}	average power consumed by subject

Q	current position vector
Q_{TARGET}	target position vector
s	laplace domain variable
$T(s)$	transfer function
$U(Q)$	total potential field
$U_{ATT}(Q)$	attractive field
$U_{REP}(Q)$	repulsive field
v	actual velocity
V	actual velocity
$V(s)$	laplace transformations of v
v_{des}	desired velocity
v_{ref}	reference velocity
V^{ave}	average velocity of the cart
$V_{ref}(s)$	laplace transformation of v_{ref}
V_{REF}	reference velocity
W	parking width
W_H	wrench applied by human
W_R	wrench applied by robot
$Y(s)$	admittance controller
$Z_H(s)$	impedance of human arm
α	integration constant
Δt	sampling time
η	relative force contribution of the robot to the task
$\rho_{TARGET}(Q)$	Euclidean distance to target
θ	angle between the human force vector and the x-axis of robot
τ_a	admittance time constant
τ_a^{opt}	optimum admittance time constant
ξ	positive constant scaling factor

Chapter 1

INTRODUCTION

Human and robot, working together, are expected to play an important role in the foreseeable future. The increasing demand for high-quality and more flexible systems to carry out complex tasks put this dyad firmly in the field. Integrating human's dexterity and problem-solving skills along with robot's precision, strength, and repeatability into tasks involving physical interaction between them, pHRI, could be quite beneficial. Such a collaborative interaction may result in significant improvements in task performance and reduction in physical human effort [1]-[6].

In order to make pHRI more effective, we need robots to anticipate the human partner's intentions and act accordingly [7]. In this regard, one of the sensory channels that flourish in nowadays is haptics [8]. For example, if we consider a collaborative object manipulation task (see Figure 1.1), the direction of force applied by human operator can be used to set the intended direction of object movement, while its magnitude can be used to regulate the movement speed of the object by robot.

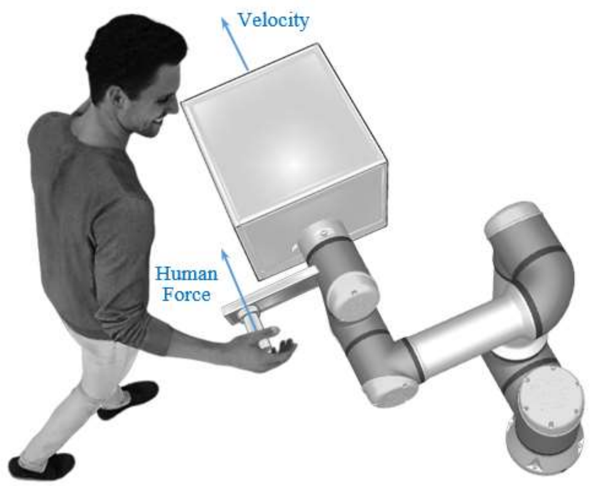

Figure 1.1: Human-robot co-manipulation scenario.

To this end, interaction controllers (admittance or its reciprocal, impedance controllers) are commonly utilized to regulate the physical interaction between human and robot. In general, it is more natural to utilize admittance controller when robots used in pHRI do not possess high back drivability and force control. As such robots are usually motion-controlled, the force applied by human can serve as the input to admittance controller, which computes the reference motion trajectory for the manipulated object in collaboration with the robot.

Although admittance controllers have been used in pHRI studies in the past, the use of a standard admittance controller in which controller parameters are fixed has some limitations. A standard admittance controller may not be flexible enough to the changes in human intentions and task requirements, which happen frequently during the execution of a collaborative task. The changes in human intention due to varying requirements of a task typically suggest that human expects either more resistive or more compliant behavior from robot. For instance, collaborative manipulation of an object typically involves three main phases, which demands different behaviors from robot in those phases; human initializes the motion (i.e., starting phase), guides the robot to bring the object closer to a target location (i.e., driving phase), and then precisely positions it to park at that location (i.e., parking phase). Initially, the task requires a rapid reaction from the robot while avoiding a jerky behavior, hence, an admittance controller having moderate dissipation capacity might be more desirable at this stage. Thereafter, during driving the manipulated object, lower dissipation capacity is preferred to promote acceleration, and hence to reduce the overall task duration and human effort. Following, as the object gets closer to the target location, increasing the dissipation gradually is needed to decelerate the object. While parking the object, maximizing the precision is more critical than reducing human effort. Human operator naturally stiffens her/his arm muscles to park the object precisely, which may degrade the stability of pHRI. In this phase of the task, if the controller parameters are adjusted to dissipate more energy, not only the stability but also the parking precision is improved.

Consequently, an adaptive admittance controller where controller parameters are no longer fixed may adapt better to varying needs of human operator in pHRI. However, as the physical strength of human is limited in performing some pHRI tasks such as manipulating heavy objects, it is required to further exploit robot’s strength. In such a case, human applies some force to the object for guidance, while robot scales up this force to help with its manipulation [9], [10]. On the other hand, in some other applications, such as robot-assisted microsurgery, where only small forces are expected to be applied to the manipulated object, human force attenuation is desired [11].

The research in pHRI have mainly focused on human intentions to regulate the interactions between human and robot. However, in the foreseeable future, as more sophisticated AI techniques are expected to be integrated into robotic systems, robots collaborating with humans are expected to have their own intentions. In such a scenario, if the intentions of a robot do not match with those of the human, there will be a conflict between them [12]. For instance, consider a robot which proactively contributes to a co-manipulation task performed with a human partner. If they have a joint intention to push the manipulated object toward the same target, they will work harmoniously with minimal conflict. This harmonious interaction enables human to spend less effort during the task. However, if human suddenly changes the target location by altering the direction of movement or parking the manipulated object before/after the initial target location while the robot keeps moving toward it, conflicting behaviors arise. Such behaviors create undesired interactions, which make the task more tiring for the human partner unless the robot recognizes these conflicts and reacts to resolve them.

Based on what we have introduced above, to regulate the interaction between human and robot in the co-manipulation task, we focus in this dissertation on 1) estimating human intention while paying attention to the requirements of the manipulation task, and 2) the dyadic interaction between human and robot partners to detect if they both have same intention to manipulate the object toward the same goal or they conflict each other.

1.1 Related Work

In physical human-robot interaction pHRI, a considerable amount of research has been directed toward detecting human intentions to regulate the interactions between human and robot. Many of the earlier studies implemented rule-based methods, while more recent ones employed ML techniques. In this regard, we review the existing literature based on these two groups of studies.

1.1.1 Rule-Based Approaches

In rule-based approaches, a set of rules based on magnitude/threshold of kinematic or kinetic variables are defined to detect human movement intention and regulate an interaction controller for intuitive pHRI. For instance, Ikeura et al. [13] utilized the velocity of manipulated object to alter the damping parameter of a variable admittance controller. In their approach, if the magnitude of object velocity was higher (lower) than a threshold value, human was assumed to speed up (slow down), and hence, the admittance damping was set to a low (high) value to promote (damp) the motion. Kang et al. [14] used object velocity to estimate human intention as to accelerate (decelerate) the object. Accordingly, when human force exceeded a certain threshold value, admittance damping was decreased (increased) as the object velocity increased (decreased). Tsumugiwa et al. [15] and Rahman et al. [16] estimated human arm stiffness and adjusted the admittance damping on-the-fly in proportion to the estimated stiffness and depending on some specific velocity thresholds. Based on the measurement of human arm muscle activation via EMG sensors, human intention was also estimated, and parameters of an interaction controller were altered accordingly to provide effective assistance in co-manipulation tasks [17], [18]. Keemink et al. [19] proposed a position-dependent admittance damping for co-manipulation of heavy objects and investigated its effect on the accuracy of object positioning, reaching time, and magnitude of force applied by human. Starting from a low value, they increased the damping between starting and target locations as a linear function of position. The methods suggested in [13]-[16], [19] relied on either some velocity or force thresholds, or position of the manipulated object, which are task-dependent information, restricting the practical use of such methods. Also, the estimation of human arm stiffness in [15] and [16] requires additional computational effort, which is not trivial if pHRI task is complex. Similarly, utilizing EMG sensors for intent detection is not very practical [17], [18] since it requires to attach them to user's arm.

There are several studies in the literature utilizing the force-based information to infer the human intention as well. For instance, Li et al. [20], [21] utilized force applied by human to interpret human intention to adjust the controller parameters accordingly. In their approach, damping was increased to improve accuracy (decreased for more compliance), when the human force was small (high). Wojtara et al. [22] implemented an interaction controller that allows a robot to follow the human partner's movement during a collaborative manipulation task based on the forces applied by the human on the object and the position of the human grasp point. Duchaine and Gosselin [23] and Duchaine et al. [24] utilized the derivative of the force applied by human and the velocity of manipulated object together to predict whether human intends to accelerate or decelerate the object. Aydin et al. [25] improved the approach proposed in [23] by adding a fuzzy-based intention estimator. Instead of using the derivative of interaction force, Lecours et al. [26] preferred the acceleration output of admittance controller directly, so that the noise in force measurement would not adversely affect the intention estimation. They used the admittance acceleration in tandem with the velocity of manipulated object to estimate whether human intends to accelerate or decelerate the object. Dimeas and Aspragathos [27] proposed a fuzzy-based online adaptation technique that utilizes the end-effector velocity of robot and force applied by human to alter the admittance damping. In [23]-[27], admittance damping was increased or decreased when the human intention was estimated as deceleration or acceleration, respectively.

In some pHRI applications, researchers have relied on amplification (attenuation) of human force to increase (decrease) the contribution of robot to the collaborative task [11], [28]-[30]. A well-known example in this group is exoskeletons [9], [31]-[33] which are designed to amplify human force. This approach has applications in different domains including rehabilitation, military, and industry. In the studies listed above, amplification (attenuation) is achieved by first scaling up (down) the forces applied by human and then feeding it to an admittance controller to generate a velocity command for the robot interacting with the environment. However, force scaling approaches used in those studies typically utilize constant amplification/attenuation gain. We believe that an adaptive force scaling, based on human intention, may result in improvements in task performance for pHRI tasks that involve even no contact interactions with an environment such as collaborative manipulation of objects.

Rule-based approaches are also used to estimate human intention to exchange roles, such as between leadership and followership. For example, Oguz et al. [34] and Kucukyilmaz et al. [8] proposed mechanisms for dynamic role exchange between the human and the robot during a collaborative task. In these studies, the authors inferred human intentions based on the forces applied by her/him on the manipulated object to adjust the robot's role in the collaborative task. Later, Mörtl et al. [35] extended these methods to work with robots on a table co-manipulation scenario. They developed a rule-based strategy based an agreement criterion regarding measured and planned human forces applied on the object, where robot and human partners dynamically exchange their roles and adjust their contributions to the task. Khoramshahi and Billard [36],[37] proposed dynamical system approaches in pHRI using human intended motion velocity to switch between different tasks, and to change robot's role between an autonomous (i.e., a stiff) leader or a compliant follower to a human partner. Although these studies demonstrate switching behaviors between active/passive roles, they do not perform harmony/conflict detection as done in this dissertation.

1.1.2 Machine Learning-Based Approaches

The emergence of machine/deep learning techniques has encouraged the researchers in pHRI to detect human intentions using data/model-driven approaches. Townsend et al. [38] trained an artificial neural network (ANN) model to predict the future human velocity based on the past velocity and acceleration using the data collected from human dyads in a co-manipulation task. This model was then validated on a table carrying task executed by a human and robot dyad. Whitsell and Artemiadis [39] presented a controller that enables humans to take the leadership on any axis they desire while manipulating an object with a robot. They utilized force and torque data as inputs to a reinforcement learning algorithm to predict the value of future rewards to activate or deactivate the robot in the desired axis. Ge et al. [40] used the force, velocity, and position measured at the interaction point between the robot arm and human upper limb as inputs to an ANN model to estimate human motion intention which is defined as the desired trajectory of human upper limb. Based on this model, Li and Ge [41] developed an adaptive interaction controller that utilized the estimated human motion intention to enable a robot to actively collaborate with a human partner instead of passively following her/his forces.

Guler et al. [42] trained an ANN classifier to detect the subtasks intended to be executed by the human operator during a collaborative drilling task. They adapted the control parameters of an interaction controller of robot based on the detected subtask to improve task efficiency. The results of the experimental study conducted with 12 participants showed that the proposed subtask classifier reduces the human effort by 20% and drilling oscillations by 25%. Lu et al. [43] utilized a LSTM model to estimate human motion intention as the desired trajectory based on human limb dynamics in a human-robot collaborative task. Moreover, a reinforcement learning algorithm was implemented to adjust one of the parameters of an interaction controller in real-time based on the estimated human intention. Ly et al. [44] trained a Deep Q-Network to estimate human intentions to reach pre-learned motion trajectories and provided adaptive haptic guidance on a robotic sorting task. Chien et al. [45] proposed a fuzzy RBF approach to estimate human hand impedance and an ANN model to estimate human motion intention, which is used to generate a reference trajectory, to compute the compensation force that assists the robot in following the intended trajectory. Wang et al. [46] estimated human intention in human-robot hand-over tasks. In their approach, they utilized an inertial measurement unit (IMU) and eight EMG sensors attached to the human forearm to measure arm motion along with muscle activity. These data were used as inputs to the extreme learning machine (ELM) algorithm to predict human hand-over intention. Sirintuna et al. [47] used EMG signals to detect the movement direction intended by human using an ANN model to constrain the movement directions using an interaction controller. They showed that this approach reduces the motion errors during collaborative positioning task executed with a robot.

Madan et al. [48] and Al-Saadi et al. [49] defined a set of interaction behaviors that are typically encountered during the co-manipulation of an object by human dyads. These interaction behaviors emerged because of partners' agreement/disagreement during the collaborative manipulations. Utilizing haptic and velocity data in [48] and haptic data solely in [49] as inputs to a ML algorithm, these behaviors were recognized offline successfully. Later, Kucukyilmaz and Issak [50] showed that these behaviors can be recognized successfully during real-time collaboration.

1.2 Contributions

In earlier pHRI studies [13]-[27], adaptive approaches based on human intention have been investigated to alter parameters of an interaction controller. In those studies, human intent has been typically interpreted as “acceleration” or “deceleration” without paying sufficient attention to different phases of a pHRI task (i.e., sub-tasks). However, as explained earlier, each phase of a pHRI task requires different actions from the controller, so the desired behavior under the specific phase can be achieved. Therefore, in the first part of this dissertation, we argue that adaptive scaling of human force based on not only the human intention but also the task phases, such as starting, driving, and parking in object manipulation, would further enhance the quality of pHRI.

Although there are several studies in the pHRI literature aiming to reduce human effort and task performance, to our knowledge, adaptive scaling of human force using an admittance controller has not been proposed for collaborative manipulation of a heavy/bulky object. In our approach, human intention as to accelerate or decelerate a manipulated object is estimated by a rule-based approach and converted to a quantitative index using a fuzzy logic scheme. This index is then integrated over time to accommodate the different requirements of each manipulation phase. Finally, the integrated value at each time step is used to alter the gain of an admittance controller on the fly for adaptive scaling of human force.

Using the proposed approach, we investigate a) if there is an optimal admittance time constant that maximizes human force amplification and b) if the resulting admittance gain profile leads to a further enhancement in a co-manipulation performance than the ones suggested in the literature.

In the second part of this dissertation, we aim to transfer the knowledge gained from human dyads [48]-[50] to a human-robot dyad. To this end, we trust that the identification and resolution of conflicts is a key skill that a robot needs to be equipped with to execute co-manipulation tasks with a human. We utilize features extracted from haptic data only to build a ML classifier that enables the robot to predict interaction behaviors and resolve conflicts when necessary. In our approach, the robot contributes to the co-manipulation task proactively when the partners work in harmony or follows the human when there is a conflict in the partners' intentions.

1.3 Outline

The rest of this dissertation is organized as follows:

Chapter 2 presents the proposed adaptive human force scaling via admittance controller for pHRI. Section 2.1 introduces the admittance controller architecture utilized in this study. Section 2.2 presents the proposed adaptation approach including the estimation of human intention index and how this index is used to modulate the gain of an admittance controller to adjust the contribution of robot to the task. The stability limits for the coupled system, the permissible range for the force amplification, and the selection of optimal time constant for the admittance controller are all discussed in Section 2.3. Section 2.4 presents the details of a pHRI experiment involving Fitts' reaching movement task, which was conducted to investigate the potential benefits of the proposed approach. Section 2.5 summarizes the experimental results and provides a discussion of the study.

Chapter 3 introduces the conflict resolution strategy during human-robot co-manipulation. Section 3.1 presents the proposed approach including the hardware setup, control architecture, and the trajectory generation method. The training and the validation experiments are introduced in Section 3.2. This section describes the training scenarios, participants and protocol, haptic features and classifier design, and the summery of the experimental results and their discussions.

Finally, conclusions and future research directions are given in Chapter 4.

Chapter 2

ADAPTIVE HUMAN FORCE SCALING VIA ADMITTANCE CONTROL FOR PHYSICAL HUMAN-ROBOT INTERACTION

In this chapter, we propose an approach for human force scaling to adaptively change the contribution of robot to a collaborative manipulation task in order to improve the task performance. In our approach, movement intentions of human are estimated from measured human force and velocity of manipulated object and converted to a quantitative index using a fuzzy logic scheme. This index is then utilized as a variable gain in an admittance controller to scale up/down the force applied by robot to the object. In essence, such an approach is similar to the adaptive admittance controller, but here, the gain contribution of the controller, not just the parameters of it, is varied. In order to adjust the contribution of robot, a frequently utilized approach in literature is to alter the dissipation capacity of the admittance controller by varying the admittance damping, but this also affects the time constant of the controller. On the other hand, our approach allows to change the gain contribution of the controller alone without changing its time constant. Therefore, the proposed approach enables a direct control of both the gain and time constant of an admittance controller, which provides flexibility in achieving different goals at different stages of a pHRI task, leading to an improvement in overall task performance.

2.1 Control Architecture

In our approach, we assume that human and robot are coupled as shown in Figure 1.1 and manipulate an object together. The admittance control architecture suggested for this purpose is depicted in Figure 2.1. Here, human exerts a force to move the object with a desired velocity v_{des}. The force applied by human f_H is measured by a force sensor, amplified by a gain G_H and then sent to the admittance controller $Y(s)$ of robot to adjust its contribution to the task. The admittance controller outputs a reference velocity v_{ref} for the motion controller of robot.

The inner motion controller of robot transmits sufficient torques to its joints to move the object with a velocity of v. We assume that robot motion controller is robust enough such that the actual velocity of the robot v is not significantly affected by environmental forces [51], [52]. Then, the transfer function $T(s)$ of the main pHRI closed-loop system in Figure 2.1 is given by:

$$T(s) = \frac{V(s)}{F_H(s)} = \frac{G_H Y(s) G(s) H(s)}{1 + G_H Y(s) G(s) H(s) Z_H(s)} \tag{2.1}$$

where $V(s)$ and $F_H(s)$ are the Laplace transformations of v and f_H, respectively. Here, $H(s) = (0.1122\, s + 31.75)/(s + 31.75)$ represents the model of a low pass filter applied to the measured human force, $Z_H(s)$ represents the impedance of human arm, and $G(s) = V(s)/V_{ref}(s)$ is the transfer function for robot [52], where $V_{ref}(s)$ is the Laplace transformation of v_{ref}. Note that all the variables introduced in this chapter are scalars as the study focuses on a 1D co-manipulation task (see Section 2.4).

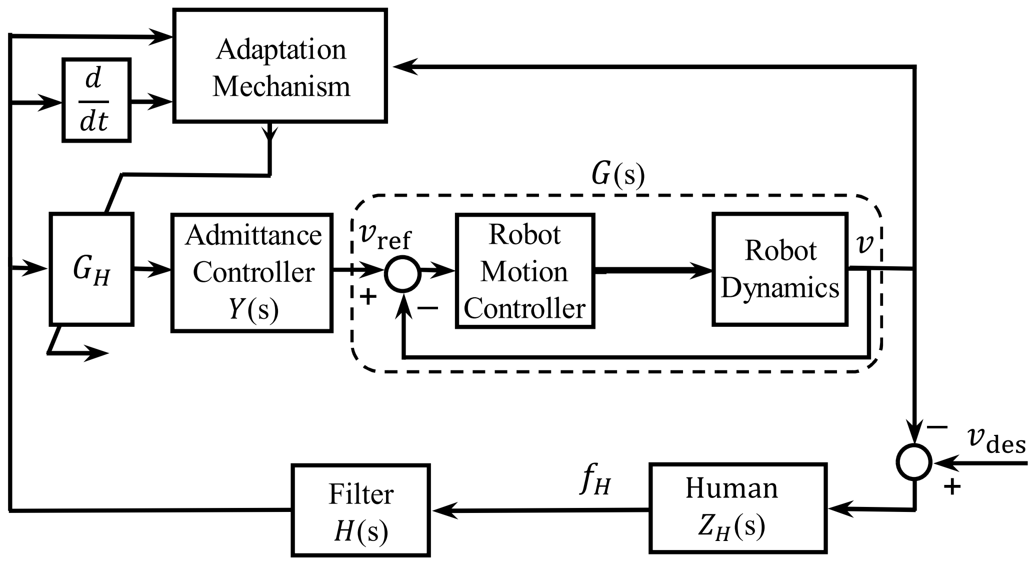

Figure 2.1: Control architecture for the pHRI system.

2.1.1 Admittance Controller

In typical implementation of an admittance controller for a pHRI task involving a collaborative object manipulation, a linear model of the following form is utilized (note that a spring element is not preferred as it forces the robot to return to an equilibrium position, which is not desirable):

$$Y(s) = \frac{V_{\mathrm{ref}}(s)}{F_H(s)} = \frac{1}{m_a s + b_a} \tag{2.2}$$

where m_a and b_a represent the admittance mass and damping, respectively. Eq. (2.2) can be rearranged as,

$$Y(s) = \frac{K_a}{\tau_a s + 1} \tag{2.3}$$

where, $K_a = 1/b_a$ is the admittance gain and $\tau_a = m_a/b_a$ is the admittance time constant. In this study, we alter the admittance gain to adjust the contribution of the robot to the task while keeping the time constant of the controller unchanged. Note that increasing (decreasing) the admittance gain decreases (increases) the energy dissipation of the controller. Tuning of admittance parameters with constant ratio of m_a/b_a has been proposed in [26], but we investigate its optimum value in this study.

2.2 Approach

Recalling the co-manipulation scenario discussed earlier, different control actions should be considered for each phase of the task. To further illustrate these phases, we consider a one-dimensional co-manipulation task. We assume that human operator and a robot collaboratively transport an object having high inertia along a straight path from a starting position to a target position which is unknown to the robot a priori. Utilizing the control architecture given in previous section, robot manipulates the object under the guidance of forces applied by the human operator. For such a task, representative profiles for the velocity of manipulated object, force applied by human, and its derivative are depicted as

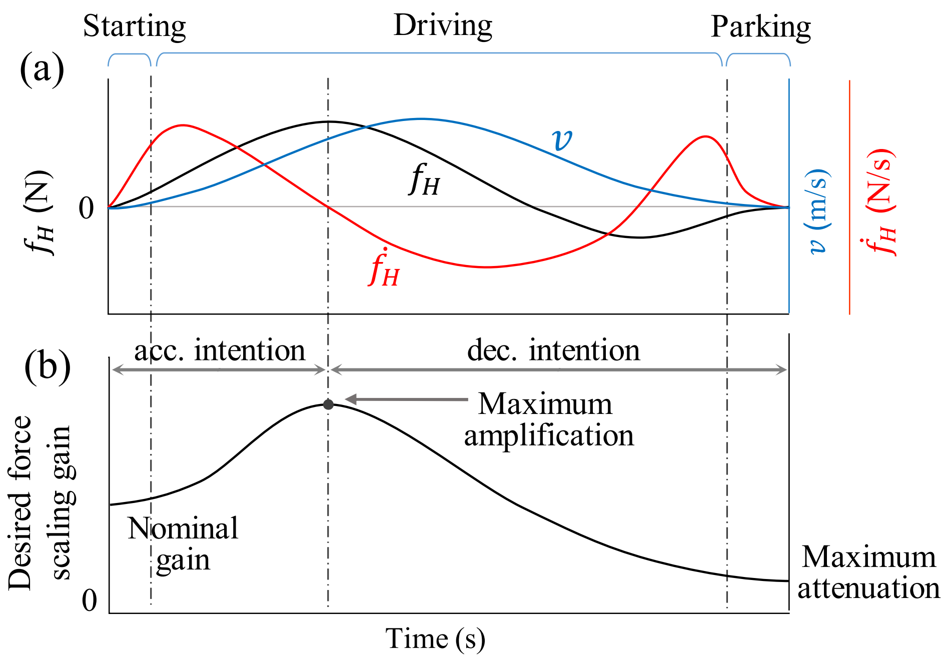

Figure 2.2: a) Representative profiles of object velocity v, force applied by human f_H, and its derivative $\dot{f}_H$, and b) desired force scaling gain profile for a co-manipulation task.

functions of time in Figure 2.2a. As anticipated, there is a phase delay between force and velocity when the inertia of the object is relatively high. For the same reason, when such an object is already in motion, reversing the force direction to decelerate it requires additional human effort.

Considering Figure 2.2a, if velocity is close to zero, velocity and force vectors are both in the same direction, and also force rate (i.e., derivative of force) is increasing in the same direction, we can argue that human intends to initialize the movement to accelerate the object (i.e., starting phase). When the velocity is sufficiently high, we can say that driving phase is being executed. If the velocity is close to zero again but force and force rate are in opposite directions, we can assume that human intends to park the object to the target location. Based on the description above, one can carefully design a profile for the admittance gain to satisfy the requirements of each phase. Such a profile is given in Figure 2.2b. The gain starts from a nominal value and increases slowly during the starting phase. In the driving phase, the dissipative (i.e., resistive) behavior of robot should be avoided as human desires to accelerate the object easily. At some point during this phase, human intends to decelerate the object (note that if the object has large inertia, it may continue to accelerate as in Figure 2.2a; force magnitude starts to decay indicating human desires to decelerate the object though the velocity continues to increase). From this point on (see the maximum amplification point in Figure 2.2b), the dissipation capacity of the controller should be increased based on how much human intends to decelerate.

In order to achieve a gain profile similar to the one proposed in Figure 2.2b, we first estimate human movement intention as to accelerate or decelerate using a rule-based approach and then quantify it by a numerical value using a fuzzy logic scheme. We then integrate this value along the movement trajectory while bounding it by a logistic sigmoid function to comply with the different requirements of each task phase.

2.2.1 Estimation of Human Intention

In earlier studies, either velocity of the manipulated object and the derivative of force applied by the human [23]-[25] or velocity and force [27] were used to estimate human intention as to either accelerate or decelerate the object. In our approach, we utilize all three of them to estimate human intention and quantify it by a numerical value called as Human Intention Index (K_{HII}). All three are needed to carefully detect the human intention during the driving phase, especially when manipulating a heavy object at a high speed. Towards the end of this phase, human reverses the force direction to dissipate the generated kinetic energy in order to park the object successfully without an overshoot in the next phase. If we use force derivative and velocity only, then human intention would be detected incorrectly as acceleration during the parking phase (Figure 2.2a). On the other hand, if we use force and velocity only, then the detection of deceleration intention will be delayed.

Figure 2.3a shows our approach for estimating human intention. First, the features are fed to a fuzzy logic scheme which generates K_{HII}. This scheme outputs a value representing human intention as to accelerate ($0 < K_{\mathrm{HII}} \leq 1$) or decelerate ($-1 \leq K_{\mathrm{HII}} < 0$) the manipulated object. Each input and the output consist of three normalized triangular membership functions (positive, intermediate, and negative). The Mamdani fuzzy inference system is utilized, and the intention rules described in (2.4) are

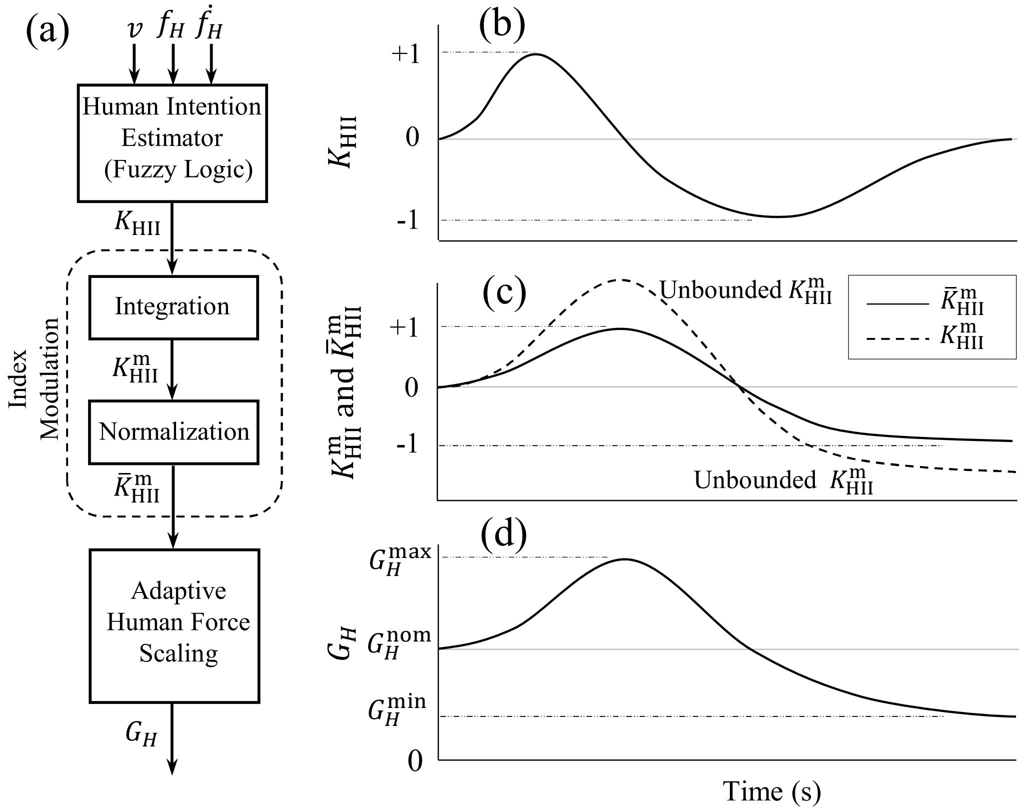

Figure 2.3: a) Proposed adaptation mechanism, and the representative profiles for b) human intention index K_{HII}, c) integrated ($K_{\mathrm{HII}}^{\mathrm{m}}$) and bounded ($\bar{K}_{\mathrm{HII}}^{\mathrm{m}}$) human intention indices, and d) desired gain (G_H).

implemented. Table (2.1) provides more details about how these rules were extracted and utilized in the fuzzy logic scheme. A representative profile of K_{HII} as a function of time is depicted in Figure 2.3b.

$$
\begin{aligned}
&v.\dot{f}_H > 0 \quad &&\Rightarrow \begin{Bmatrix} v.f_H > 0 \Rightarrow \text{Intent: acc.} \\ v.f_H < 0 \Rightarrow \text{Intent: dec.} \end{Bmatrix} \\
&v.\dot{f}_H < 0 \quad &&\Rightarrow \{\text{Intent: dec.}\} \\
&v.\dot{f}_H \approx 0 \quad &&\Rightarrow \{\text{no change in intent}\}
\end{aligned}
\tag{2.4}
$$

Table 2.1: Human intention rules utilized in the fuzzy logic scheme.

Rule number	Inputs			Output
	$v(t)$	$\dot{f}_H(t)$	$f_H(t)$	$K_{\mathrm{HII}}(t)$
1	+	+	+	+
2	+	+	−	−
3	−	−	+	−
4	−	−	−	+
5	+	−	+	−
6	+	−	−	−
7	−	+	+	−
6	−	+	−	−
7	≈ 0	+	+	$K_{\mathrm{HII}}(t-1)$
8	≈ 0	+	−	$K_{\mathrm{HII}}(t-1)$
9	≈ 0	−	+	$K_{\mathrm{HII}}(t-1)$
10	≈ 0	−	−	$K_{\mathrm{HII}}(t-1)$
11	+	≈ 0	+	$K_{\mathrm{HII}}(t-1)$
12	+	≈ 0	−	$K_{\mathrm{HII}}(t-1)$
13	−	≈ 0	+	$K_{\mathrm{HII}}(t-1)$
14	−	≈ 0	−	$K_{\mathrm{HII}}(t-1)$

A further processing on K_{HII} is needed to obtain the desired gain profile depicted in Figure 2.2b. To this end, a simple discrete integration of K_{HII} is a practical solution.

Note that derivative of force, which is typically noisy, is utilized in the computation of K_{HII}, hence such integration accumulates the index values on-the-fly, producing a profile that is not only similar to the desired gain profile but also robust to noise.

Hence, the integrated human intention index is obtained using the following equation:

$$K_{\mathrm{HII}}^{\mathrm{m}}(t) = K_{\mathrm{HII}}^{\mathrm{m}}(t-1) + K_{\mathrm{HII}}(t)\,\alpha\,\Delta t \tag{2.5}$$

where, α is the integration constant used to control the rate of accumulation and to reduce the delay in gain adaptation, and Δt is the sampling time.

Due to the integration process, $K_{\mathrm{HII}}^{\mathrm{m}}$ might reach to large values. A logistic sigmoid function is utilized in this study to obtain a bounded value as (see Figure 2.3c):

$$\overline{K}_{\mathrm{HII}}^{\mathrm{m}}(\mathrm{t}) = -1 + 2\left(\frac{1}{1+\mathrm{e}^{-K_{\mathrm{HII}}^{\mathrm{m}}(\mathrm{t})}}\right) \tag{2.6}$$

2.2.2 Adaptive Human Force Scaling

In our design, when the operator intends to accelerate the object, the force scaling gain G_H, which is applied to the measured human force to adapt the contribution of robot to the co-manipulation task, increases from its nominal value G_H^{nom} until reaching to its maximum allowable limit G_H^{max} (i.e., $G_H^{\mathrm{nom}} \le G_H \le G_H^{\mathrm{max}}$). Hence, more assistance is provided to human during acceleration. When deceleration intention is detected, G_H decreases from its current value toward the minimum limit G_H^{min}, which is below the nominal value (i.e., $G_H^{\mathrm{min}} \le G_H < G_H^{\mathrm{nom}}$). In order to make the transition smoother, the scaling gain is calculated as (see Figure 2.3d):

$$G_H(t) = G_H^{\mathrm{nom}} + I_H\,\overline{K}_{\mathrm{HII}}^{\mathrm{m}}(\mathrm{t}) \tag{2.7}$$

Here, $I_H = \frac{\left(1+\mathrm{sgn}\left(\overline{K}_{\mathrm{HII}}^{\mathrm{m}}(\mathrm{t})\right)\right)}{2}(G_H^{\mathrm{max}} - G_H^{\mathrm{nom}}) + \frac{\left(1-\mathrm{sgn}\left(\overline{K}_{\mathrm{HII}}^{\mathrm{m}}(\mathrm{t})\right)\right)}{2}\left(G_H^{\mathrm{nom}} - G_H^{\mathrm{min}}\right)$ is the weighting factor to bound the scaling gain within the allowable limits (i.e. between G_H^{min} and G_H^{max}), where $\mathrm{sgn}(x)$ is the sign function of x.

Once the scaling gain for human force is estimated, (2.3) can be rewritten as follows:

$$Y(s) = \frac{G_E}{\tau_a s + 1} \tag{2.8}$$

where $G_E = G_H K_a$ is the effective admittance gain of the controller.

We can deduce that altering the force scaling gain G_H affects both admittance damping and inertia at the same rate, resulting no change in the admittance time constant.

2.3 Stability Limits

2.3.1 Stability

Stable interaction is mandatory for any pHRI system, but the trade-off between stability and transparency has to be balanced well for optimal task performance [53]. To ensure stability, we inspect the pole locations of the closed-loop transfer function, T(s), given in (2.1) for a range of gain (K_a) and time constant (τ_a) values of the admittance controller while keeping $G_H = 1$. For this purpose, we need the transfer function models of robot and human arm impedance. We utilize UR5 (Universal Robots Inc.) as the collaborative robot in our study. Since the manufacturer does not supply the dynamical model of the robot, we rely on the transfer function model, $G(s)$, estimated by Aydin et al. [52]. The dynamical behavior of human arm is nonlinear, time and configuration dependent. However, it is a commonly used simplifying assumption that the impedance of human arm, $Z_H(s)$, can be described by a linearized mass-spring-damper model (see [13], [51], [52]) as $Z_H(s) = m_H s + b_H + k_H/s$, where m_H, b_H, and k_H are the human arm endpoint mass, damping and stiffness, respectively. Although exact dynamics of human arm is unknown, the parameters of human arm impedance typically reside within specific limits. In light of the literature [54]-[56], the upper bound for human arm stiffness k_H is taken as 600 N/m, and the lower and upper bounds for the mass parameter m_H are taken as 0.1 and 5 kg, respectively, while the limits for the damping b_H are set to 0.1 and 41 Ns/m. For each extreme combination of parameters of human arm impedance (m_H, b_H, k_H), stable sets of controller parameters (K_a, τ_a) are computed and stability boundaries are determined. Then, as suggested in [57], [58], the parameters (K_a, τ_a) corresponding to the conservative regions, where the stability is ensured under each extreme combination of human arm impedance parameters (m_H, b_H, k_H), are considered as the stable controller parameters (see Figure 2.4). Note that these parameters are valid for the case in which the robot motion is not significantly affected by the environment (see Section 2.1).

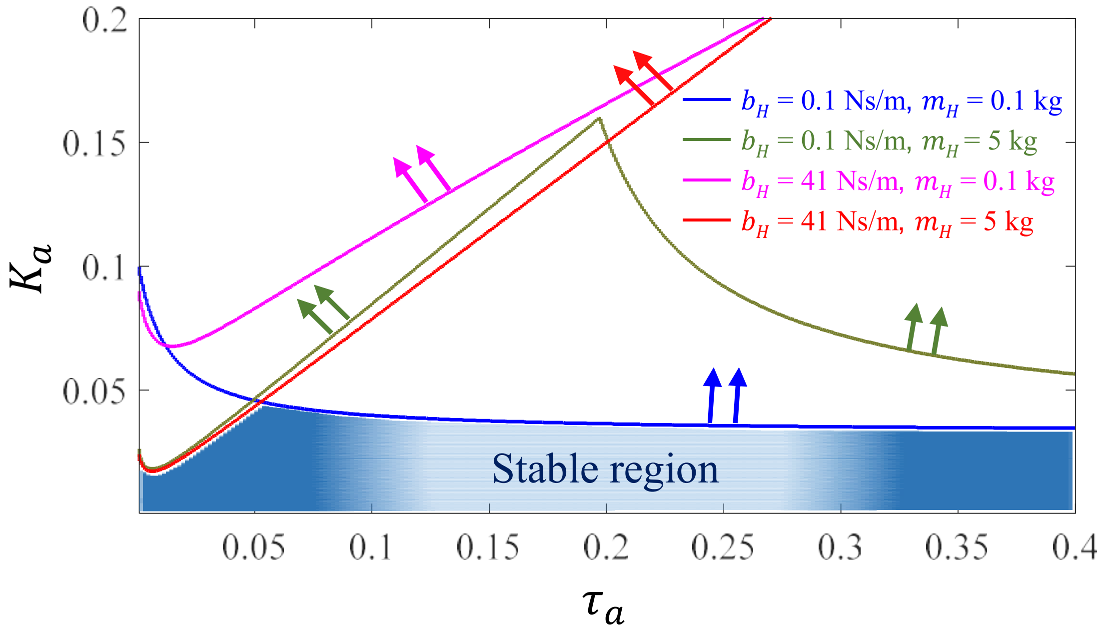

Figure 2.4: Stability maps of the pHRI system for k_H = 600 N/m. The curves represent the stability boundaries for different combinations of human arm impedance parameters m_H and b_H. The shaded area represents the sets of effective gain and time constant values that ensure stability for all bounds of m_H and b_H. Directions of the arrows refer to unstable regions for each set of m_H and b_H.

2.3.2 Maximum Amplification

In the above analysis, the stable regions of controller parameters are determined while keeping $G_H = 1$. To determine the upper bound of G_H that can be used for maximum force amplification, we investigate the gain margin of the system under each set of (K_a, τ_a) in the stable region of Figure 2.4. The contour plot of G_H values in this region is depicted in Figure 2.5. From this figure, we can observe that, for each time constant τ_a, amount of allowable change in amplification depends on the value of admittance gain K_a. Moreover, for a given K_a, there is an optimal admittance time constant, where the force amplification is maximum. In Figure 2.5, this value is $\tau_a^{\mathrm{opt}} = 0.054$, which can be used to determine the maximum allowable amplification gain, $G_H^{\max}$, and hence the maximum effective controller gain, $G_E^{\max}$. For example, let's assume that the parameters of an admittance controller are $\left(K_a, \tau_a^{\mathrm{opt}}\right)$ = (0.0167, 0.054) and the gain margin of the corresponding closed loop system is 2.68 (see point A in Figure 2.5). Hence, the maximum allowable amplification gain is $G_H^{\max} = 2.68$. Accordingly, the maximum effective controller gain is $G_E^{\max} = G_H^{\max} K_a$ = 0.0448.

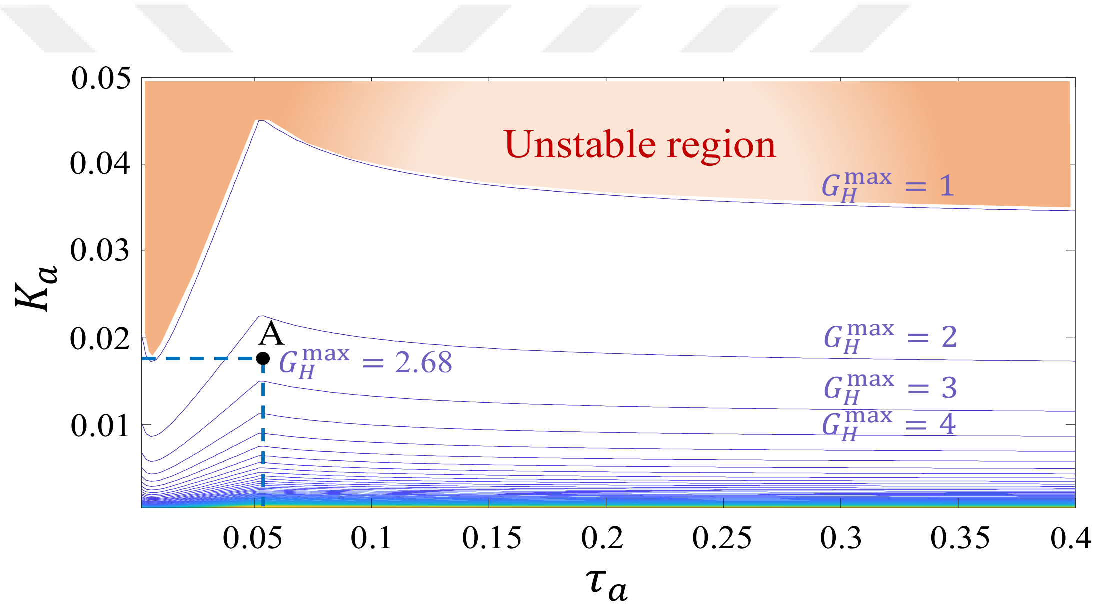

Figure 2.5: Gain margin for the sets of controller parameters (K_a, τ_a) in the stable region.

2.4 Experiment

We designed and conducted a pHRI experiment to investigate the following research questions:

Q1: Is there an optimum admittance time constant that maximizes human force amplification in pHRI for the proposed gain profile (Figure 2.2b)?

Q2: Does the proposed admittance gain profile leads to a more effective co-manipulation in terms of task performance than the ones suggested in the literature?

2.4.1 Experimental Setup

The main components of the set-up used for our pHRI experiment (see Figure 2.6) consists of a collaborative robot (UR5, Universal Robot Inc.), a mobile cart that is rigidly connected to the robot and moving on a rail and carrying a mass of 26 kg (note that the

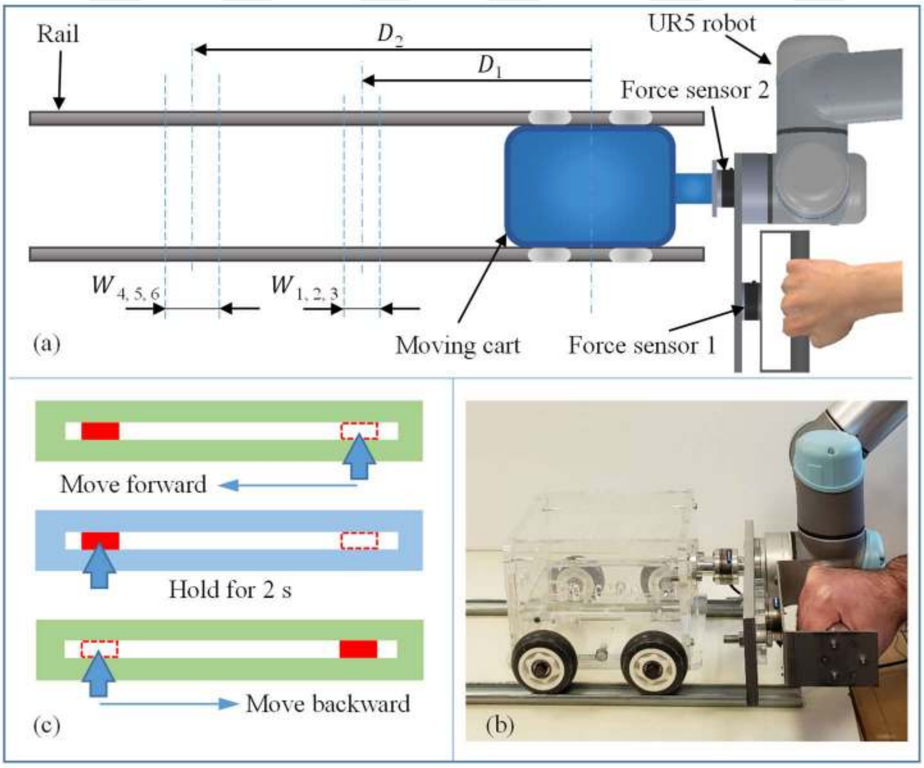

Figure 2.6: The experimental setup (a, b) and visual feedback provided to subjects during the experiment (c).

mass is not shown in Figure 2.6b), and two force sensors (Mini40, ATI Inc.), each measuring the force applied by subject and robot to the cart separately (see Figures 2.6a, 2.6b). All experimental data was acquired at 125 Hz (the update rate of the closed-loop control system shown in Figure 2.1) by a DAQ card (USB-6343, National Instruments Inc.). During the experiments, the instantaneous force applied to the cart by a subject is scaled up/down according to her/his movement intention and then fed to the admittance controller, which outputs a desired velocity for the cart. The robot aims to push the cart with this desired velocity until a new force input comes from the subject (see the control architecture in Figure 2.1).

2.4.2 Experimental Procedure

Subjects were asked to grasp the handle shown in Figure 2.6a and move the cart from a starting point to a parking zone as fast and accurate as possible. Subjects were asked to perform the task in both directions; in one trial, they pushed the cart forward, and in the successive trial, they pulled it backward. Visual feedback was provided to subjects during the experiment by displaying a moving cursor on a computer screen, emulating the movements of cart (see Figure 2.6c). Subjects were asked to hold the cart stable in the parking zone for 2 seconds. A time counter was displayed through the computer screen and triggered when they entered the parking zone for the first time. During this dwell time, if subject maintained the cart position successfully without overshooting outside the parking zone, a prompt “start to the next trial” appeared on the computer screen, and the next trial began. Otherwise, the time counter restarted at every overshoot, and the additional overshooting time was added to the movement time as a penalty.

2.4.3 Participants

Nine subjects (3 females and 6 males whose age vary between 20 and 40 with an average of 26) participated in the experiment. Subjects gave informed consent about their participation in the experiment. The experimental study was approved by the Ethical Committee for Human Participants of Koc University.

2.4.4 Experimental Design

The experiment was designed to imitate Fitts's reaching movement task [59]. Fitts's reaching task requires a rapid movement from a starting point to a target area. This task is designed specifically to investigate speed-accuracy trade-off characteristics of human muscle movement with some analogy to Shannon's channel capacity theorem. As the aim in most co-manipulation tasks such as ours is to reduce human effort while maximizing manipulation accuracy, Fitts's reaching task offers utilization of well-established measures to characterize task performance. In particular, a linear relationship between movement time MT and index of task difficulty ID has been suggested by Fitts [59], $\mathrm{MT} = a + b\,\mathrm{ID}$. The empirical coefficients a and b depend on environment and controller. The index of difficulty (in bits) is a function of reaching distance D and parking width W through Shannon formula [60], $\mathrm{ID} = \log_2(D/W + 1)$. Following these relations, we designed the experiment by considering three indices of difficulties (ID = 4, 5, and 6 bits) and two reaching distances (D = 25, and 40 cm). This results in six different parking widths as listed in Table 2.2.

Table 2.2: Fitts' task design parameters.

Parking width W (cm) = D / (2^{ID} - 1) Shanoon formula		Index of dificulty ID (bits)		
		4	5	6
Distance D (cm)	$D_1 = 25$	$W_1 = 1.667$	$W_2 = 0.81$	$W_3 = 0.4$
	$D_2 = 40$	$W_4 = 2.667$	$W_5 = 1.29$	$W_6 = 0.635$

2.4.5 Performance Measures

We used the average power consumed by subject ($P^{\mathrm{ave}} = 1/(t_f - t_i)\int_{t_i}^{t_f} |f_H(t).v(t)|\,dt$), average force applied by subject ($F_H^{\mathrm{ave}} = 1/(t_f - t_i)\int_{t_i}^{t_f} |f_H(t)|\,dt$) [51], average force applied by robot to move the cart ($F_R^{\mathrm{ave}} = 1/(t_f -$

$t_i) \int_{t_i}^{t_f} |f_R(t)|\, dt)$, average velocity of the cart ($V^{\text{ave}} = 1/(t_f - t_i) \int_{t_i}^{t_f} |v(t)|\, dt$), and the movement time MT as measures to evaluate the task performance. In the expressions above, t_i and t_f were the time when the cart velocity just exceeded 2% of the maximal velocity of the trial and the time when the cart entered the parking zone, respectively [19]. The movement time MT was quantified by measuring the time starting from t_i till finishing the trial after removing the dwell time [19].

We calculated the ratio, $\eta = F_R^{\text{ave}}/F_H^{\text{ave}}$, to evaluate the relative force contribution of the robot to the task. Moreover, to evaluate the parking accuracy, we calculated the parking overshoot, which was, for a single trial, the number of times the manipulated object left and reentered the target zone during parking before the trial was finished successfully [19]. Then, parking overshoot was computed for each subject by summing up the number of reentries for all trials of that subject for each ID divided by the total number of trials of that ID.

2.4.6 Regarding Q1: Verification of the Optimum Time Constant

As the theoretical analysis in the previous section has shown, there is an optimal time constant, τ_a^{opt}, that maximizes the amplification capacity of human force. In this section, we report the empirical evidence to support this finding. We designed an experimental study to investigate the effect of time constant on the performance of our pHRI system. In our experiment, we used an admittance controller utilizing the proposed adaptive force amplification gain profile with six different time constants, including values below and above τ_a^{opt}. These conditions are labeled as $\tau_1, \tau_2, \tau_3 (= \tau_a^{\text{opt}}), \tau_4, \tau_5,$ and τ_6, corresponding to the time constant values of 0.03, 0.04, 0.054, 0.08, 0.1, and 0.2, respectively. For a given nominal admittance gain K_a = 0.0167, the permissible maximum amplification gain $G_H^{\max}$ for each admittance time constant was obtained from the gain margin plot (Figure 2.5) as 1.78, 2.18, 2.68, 2.46, 2.37, and 2.17 for $\tau_1, \tau_2, \tau_3, \tau_4, \tau_5$, and τ_6, respectively. For all conditions, the desired profile of the adaptive controller starts from the same nominal amplification gain $G_H^{\text{nom}} = 1$ and ends at the same minimum amplification (i.e., maximum attenuation) gain $G_H^{\min} = 0.33$. Other parameters are taken as $\alpha = 20$, $\Delta t = 0.008$ s.

In this experiment, each experimental condition was repeated 8 times for each parking width W given in Table 2.2. Thus, there were a total of 288 (6 conditions x 6 parking widths x 8 repetitions) trials in the experiment. Each subject conducted the experiment in four sessions; 72 (6 conditions x 6 parking widths x 2 repetitions) trials per session. The trials of each session were randomized while the same order was displayed to each subject. In addition, subjects were given a training set of 12 (6 conditions x 2 parking widths x 1 repetition) trials prior to each session.

2.4.7 Regarding Q2: Comparing the Proposed Adaptive Gain Profile with the Other Profiles Suggested in the Literature

To investigate the potential benefits of proposed admittance controller with adaptive force scaling utilizing the proposed gain profile (labelled as C1), we compared it with two different admittance controllers; C2 and C3 (see Figure 2.7) under the same optimal time constant τ_a^{opt}. Note that K_a = 0.0167 and τ_a^{opt} = 0.054 were used as the nominal admittance parameters in all controllers. As shown in Figure 2.3d, the desired gain profile for C1 relies on three critical values; first, the nominal force scaling gain G_H^{nom}, which is the value at the start of motion. Second is the maximum force scaling gain G_H^{max}, which is obtained from the gain margin plots in Figure 2.5. The last is the minimum force scaling gain (i.e., maximum attenuation) G_H^{min}, which is used during the parking phase. In our implementation of the gain profile for C1, the values given in Table 2.3 were utilized.

Table 2.3: Parameter values for the controller C1.

(K_a, τ_a^{opt})	G_H^{nom}	G_H^{max}	G_H^{min}	α	Δt
(0.0167, 0.054)	1	2.68	0.33	20	0.008

In addition to the controller given above, we explored the effect of different gain profiles suggested in the literature on the task performance. These alternative profiles, C2 and C3, have been suggested in the literature to adjust the dissipation capacity of an admittance controller by varying the admittance damping. In C2, which was adopted from the earlier studies in [23]-[26], the amplification (attenuation) occurs only during the acceleration (deceleration) (see Figure 2.7). Although the force scaling gain varied between the maximum $G_H^{\max}$ and minimum $G_H^{\min}$ values in C2, the nominal value (i.e., G_H^{nom}) was used during both the starting and parking phases. On the other hand, C3, which was adopted from the studies in [14] and [27], represents a gain profile where high amplification was provided to the operator during the driving phase (see Figure 2.7) though $G_H^{\min}$ was used during both the starting and parking phases.

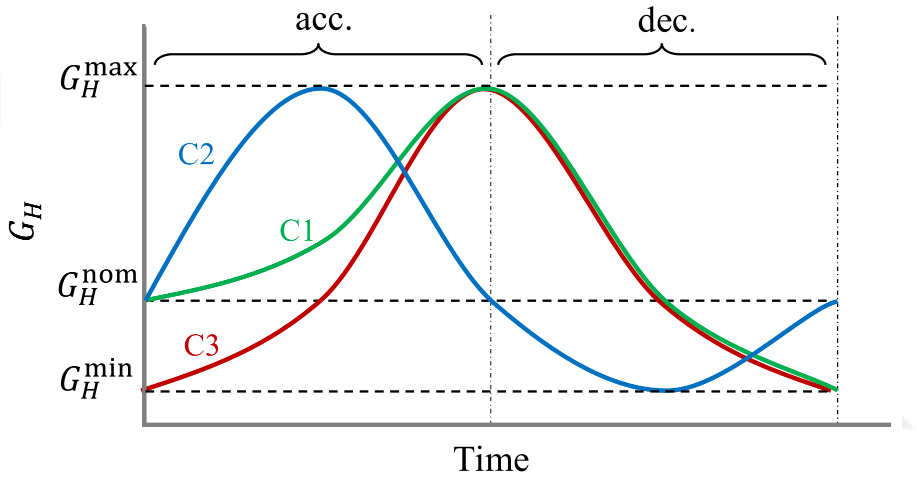

Figure 2.7: Representative gain profiles for the controllers tested in our study. C1 is the proposed adaptation gain profile, while C2 and C3 are similar to the adaptation profiles resulted from the adaptive approaches introduced in [23]-[26], and [14, 27], respectively. Please note that the gain profiles C2 and C3 for force scaling are mirror images of the damping profiles suggested in the related references.

In summary, three controllers were tested in this experiment, utilizing different adaptive gain profiles (C1, C2, and C3). Each controller case was repeated 8 times for each parking width W given in Table 2.2. Thus, there were a total of 144 (3 controllers x 6 parking widths x 8 repetitions) trials in the experiment. Each subject conducted the experiment in four sessions; 36 (3 controllers x 6 parking widths x 2 repetitions) trials per session. The trials of each session were randomized while the same order was displayed to each subject. In addition, subjects were given a training set of 6 (3 controllers x 2 parking widths x 1 repetition) trials prior to each session.

2.4.8 Data Analysis

The performance measures defined in Section 2.4.5 were computed and the means and standard errors of them were evaluated. All dependent variables (i.e., measures) were tested for normality using the Shapiro–Wilk test. We found that the distribution was non-normal for some of the measures. Normalizing transformations were applied to the measures as suggested in [61]. A two-way ANOVA was conducted to examine the effects of index of difficulty (ID) and admittance time constant (τ) regarding Q1, and controller type regarding Q2, on each performance measure. A significance level of p = 0.05 was used to test the null hypothesis in the statistical analysis.

2.4.8.1 Regarding Q1

There was a statistically significant interaction between ID and τ on parking overshoot and movement time (MT) measures. Therefore, we examined the simple main effects of ID and τ on both parking overshoot and MT. On the other hand, no significant interaction was observed between the effects of ID and τ on F_H^{ave}, η, P^{ave}, and V^{ave} measures. So, we selected the Tukey post-hoc test to investigate the effect of admittance time constant τ on these measures. The mean values of subjects for all measures are reported in Figures. 2.8 and 2.9.

2.4.8.2 Regarding Q2

In the analyses, we found a significant interaction between the experimental factors (ID and controller type) for all measures. Therefore, further analysis was performed to evaluate the individual simple main effects of ID and controller type. Figure 2.10 illustrates the results of our second experiment which was designed to compare the proposed gain profile (C1) with the ones proposed in the literature (C2 and C3).

2.4.9 Results and Discussion

2.4.9.1 Regarding Q1

Figures 2.8a, 2.8b, 2.8c, and 2.8d report the average force applied by human F_H^{ave}, the relative contribution of the robot in task execution η, the average power consumed by human P^{ave}, and the average velocity V^{ave}, respectively. These plots were obtained for each performance measure under each admittance time constant τ by averaging the results of all ID levels. Post-hoc comparisons using the Tukey test indicated that F_H^{ave} (η) under $\tau_3(=\tau_a^{\mathrm{opt}})$ was significantly lower (higher) than those of all other admittance time constants. Furthermore, P^{ave} under τ_3 was significantly lower than those of τ_1, τ_5, and τ_6. Although P^{ave} under τ_3 was lower than those of τ_2 and τ_4 as well, the difference was not statistically significant. The effect of admittance time constant on V^{ave} was not statistically significant.

As depicted in Figure 2.9a, parking overshoot under τ_3 was not significantly different than those of the others for ID = 4. Furthermore, the differences between the parking overshoots under τ_1, τ_2, τ_3, τ_4, and τ_5 were not significant for ID = 5 and ID = 6, while parking overshoot under τ_6 was significantly higher than those of the others.

Figure 2.9b illustrates the movement time MT for different IDs. MT under τ_3 was significantly lower than that of τ_6 (those of τ_1 and τ_6) for ID = 4 (for ID = 5). For ID = 6, MT under τ_6 was significantly higher than those of the others.

For each time constant, the relation between MT and ID was linear ($\mathrm{MT} = a + b\ \mathrm{ID}$) with a high R-squared value (see Table 2.4), which indicates that Fitts's law is also valid for a dissipative environment as suggested in [19]. The linear relationship between MT and ID shows that the slopes b under τ_1-τ_5 were similar (see Figure 2.9c), as listed in Table 2.4. On the other hand, the slope of τ_6 was higher since the controller under τ_6 utilizes a higher admittance time constant. Furthermore, the slope, b, is reciprocally related to the information transmission rate (i.e., index of performance). Specifically, the index of performance (i.e., $\mathrm{IP} = 1/b$) describes the information transmitted to subjects per unit time to successfully perform the task [19], [62]. As expected, IP was lower under τ_6 than those of the others since a high time constant causes sluggish response. This increases the possibility of overshooting at higher ID (see Figure 2.9a), which in turn increases task duration, and the slope. As expected, movement time MT depicted in Figure 2.9b showed that subjects completed the task significantly slower under τ_6 than those of τ_1-τ_5, especially at higher ID. Although subjects were moving in a relatively similar speed under all time constants considered in this experiment (see Figure 2.8d), they completed the task with more overshoots under τ_6 compared to those of the others, which led to longer MT.

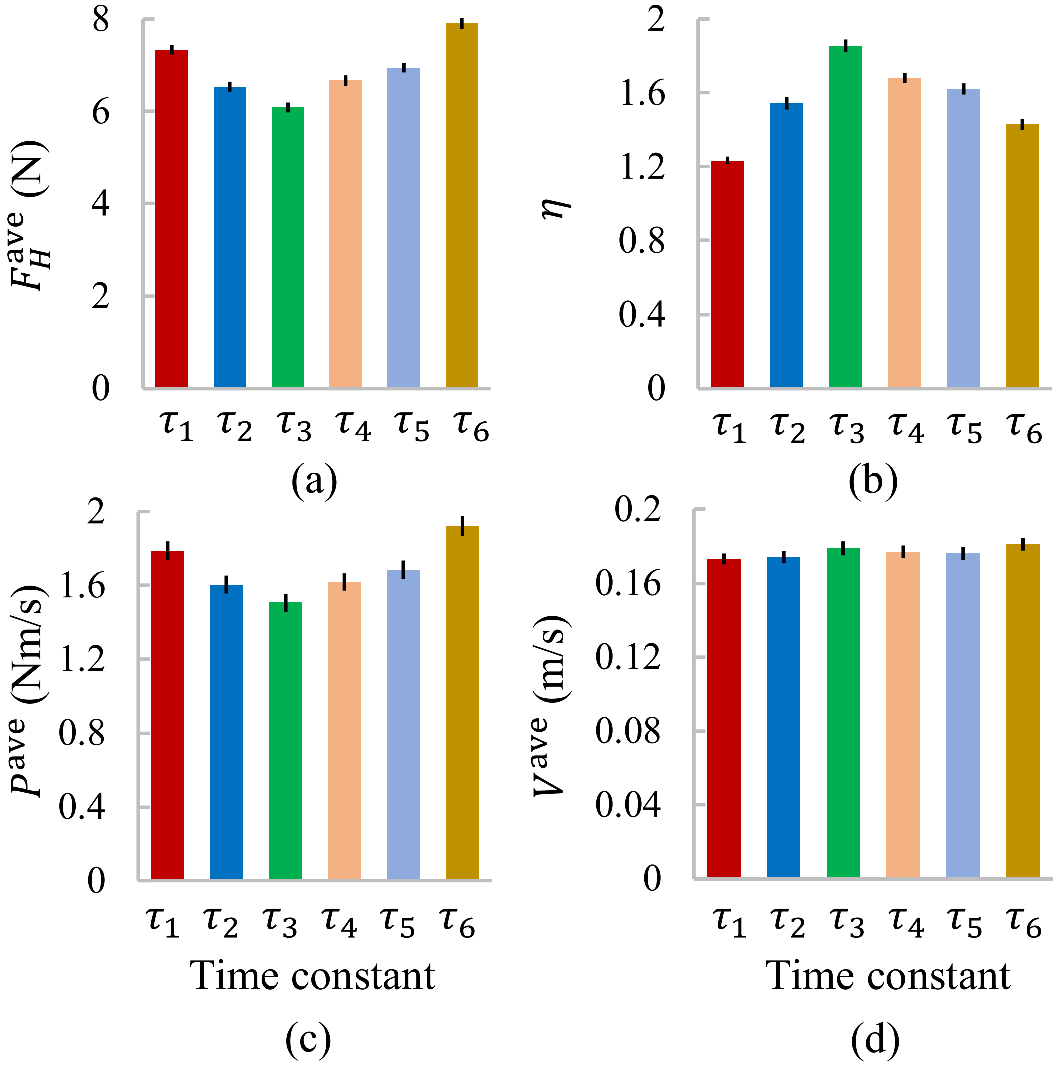

Figure 2.8: The means and standard errors of the means of the performance measures; a) average force applied by subject F_H^{ave}, b) relative force contribution of the robot η, c) average power consumed by subject P^{ave}, and d) average velocity of the cart V^{ave} for six admittance time constants τ_1, τ_2, τ_3, τ_4, τ_5 and τ_6.

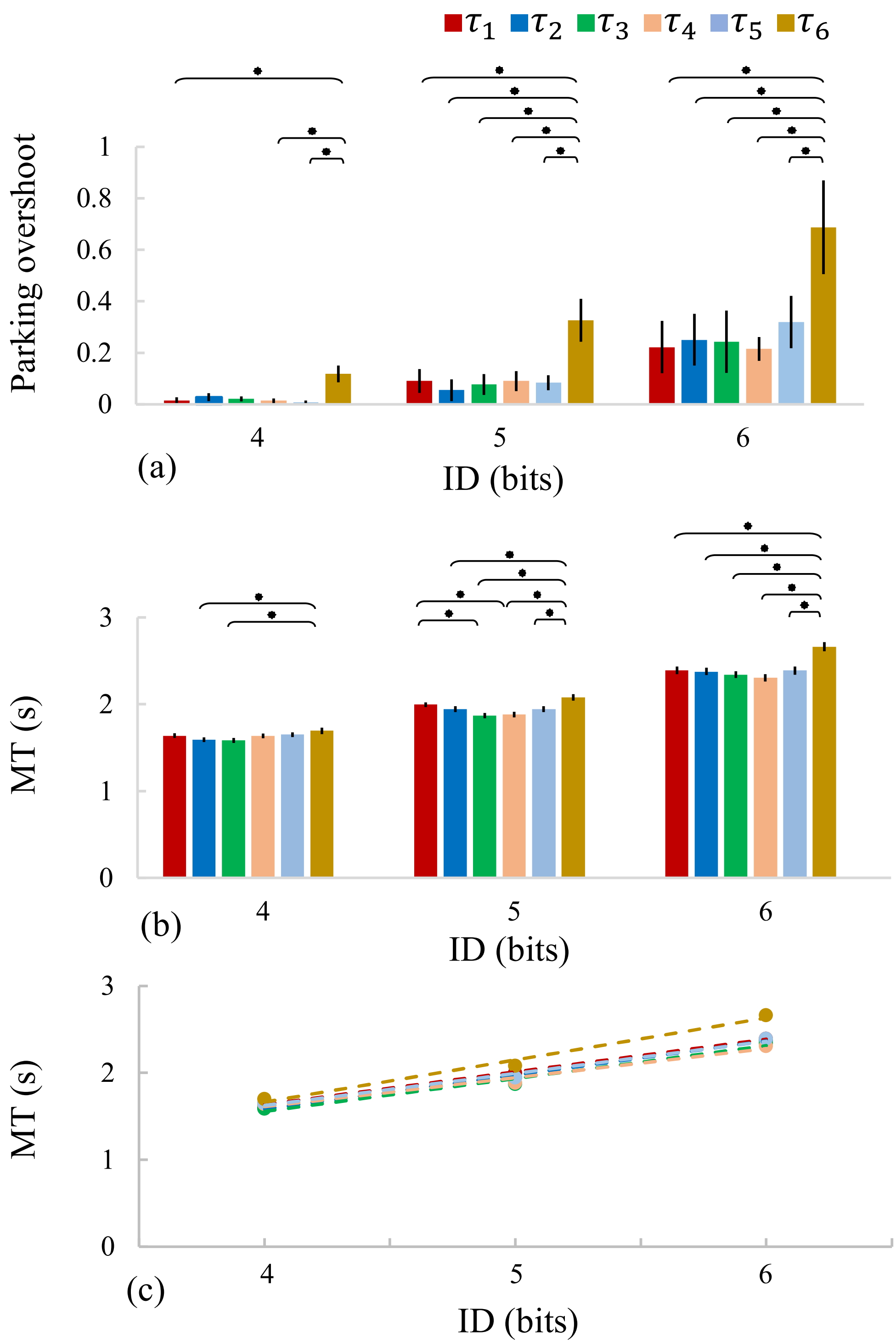

Figure 2.9: The means and standard errors of means of the performance measures; a) parking overshoot, b) MT, and c) linear regression between ID and MT for six admittance time constants τ_1, τ_2, τ_3, τ_4, τ_5, and τ_6. Horizontal bracket with * on top indicates statistical significance between the results of the two corresponding conditions.

Table 2.4: Parameters of the linear regression between MT and ID for the admittance time constants τ_1, τ_2, τ_3, τ_4, τ_5, and τ_6.

Conditions	a	b	IP (1/b)	R^2
τ_1	0.133	0.375	2.67	0.99
τ_2	0.014	0.392	2.55	0.99
τ_3	0.041	0.378	2.64	0.98
τ_4	0.273	0.334	2.99	0.97
τ_5	0.151	0.369	2.71	0.98
τ_6	- 0.266	0.483	2.07	0.98

As shown in Figures 2.8a-2.8c, τ_3 transcended τ_1, τ_2, τ_4, τ_5, and τ_6 in terms of F_H^{ave}, η, and P^{ave}. These experimental results support our theoretical analysis in Section 2.3 and our claim that there is an optimal time constant ($\tau_3 = \tau_a^{\text{opt}}$) maximizing the human force amplification.

This experiment also highlighted the difference in the performance between the conditions of low and high time constant. For instance, $\tau_2 = 0.04$ and $\tau_6 = 0.2$ have almost the same allowable force amplification of 2.18 and 2.17, respectively. However, the results depicted in Figures 2.8 and 2.9 showed that τ_2 significantly outperformed τ_6 in all performance measures since increasing the time constant reduces the response speed of an admittance controller. As a result, an object having a high inertia cannot be accelerated easily [26], requiring more effort from human operator. Furthermore, once the object is accelerated, it is difficult to decelerate it as well. Hence, overshoot during parking is unavoidable.

2.4.9.2 Regarding Q2

Figures 2.10a and 2.10c depict the average force applied by subjects, F_H^{ave}, and the relative force contribution of the robot to task, η, respectively. F_H^{ave} (η) under C1 was significantly lower (higher) than those of C2 and C3 for each ID. The average force applied by robot, F_R^{ave}, is plotted in Figure 2.10b. F_R^{ave} under C2 was significantly lower

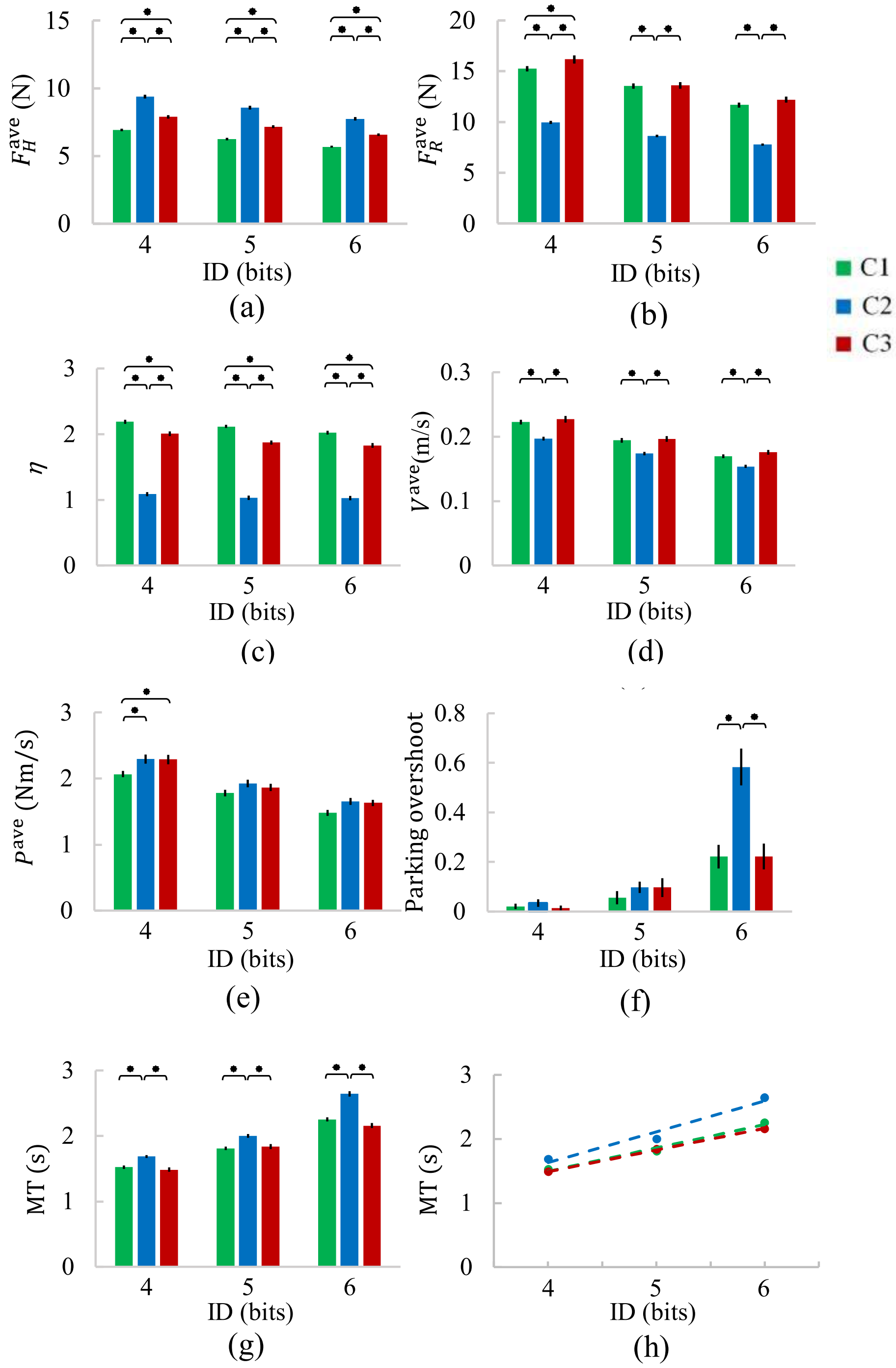

Figure 2.10: Mean values of the performance measures for three different IDs under three different controllers C1 (our proposed controller), C2, and C3. Error bars are the standard errors of means and horizontal bracket with * on top indicates statistical significance between the results of the two corresponding controllers.

than those of C1 and C3 for each ID. However, F_R^{ave} under C3 was significantly higher than that of C1 for ID = 4. The average velocity of the cart, V^{ave}, is plotted in Figure 2.10d. V^{ave} under C2 was significantly lower than those of C1 and C3. Figure 2.10e illustrates the average power consumed by subjects, P^{ave}, which was significantly lower under C1 than those of C2 and C3 for ID = 4. Figure 2.10f reports the results for parking overshoot. Parking overshoot under C2 was significantly higher than those of C1 and C3 for ID = 6. As shown in Figure 2.10g, the movement time MT under C2 was significantly higher than those of C1 and C3 for each ID.

We observed that subjects completed the task with higher MT under C2 than those of C1 and C3 for all IDs (see Figure 2.10h). This is because C2 resulted in higher dissipation than C1 and C3 (see Figure 2.7), which caused the robot to resist the movements of subjects, and hence an increase in task duration. Moreover, the index of performance IP under C2 was lower than those of C1 and C3 (see Table 2.5), which showed that less information per unit time was transmitted to subjects to perform the task successfully under C2 than those of C1 and C3.

Table 2.5: Parameters for the linear regression between MT and ID for the controllers C1, C2, and C3

Controller	a	b	IP (1/b)	R^2
C1	0.045	0.363	2.75	0.98
C2	- 0.28	0.478	2.09	0.96
C3	0.15	0.335	2.98	0.99

Figure 2.10c shows that the relative force contribution of robot to task, η, was significantly higher under C1 than those of C2 and C3 for each ID, which indicates that subjects applied less force to move the cart under C1. Figure 2.10d shows that subjects moved the cart with higher velocity under C1 and C3 than that of C2 for each ID. Since the effort made by subjects is quantified as force times velocity, subjects put significantly less effort under C1 than those of C2 and C3. Moreover, parking accuracy under C2 was

lower than those of C1 and C3 when index of difficulty was high since the gain profile of C2 ends with a non-conservative gain value (i.e., G_H^{nom}), causing a lower dissipation than those of C1 and C3. C1 and C3 allowed subjects to end the task with the maximum attenuation gain G_H^{min}, which provided more dissipation at the parking phase to position the cart accurately (see Figure 2.7).

2.5 Discussion

To summarize above, the results of the experiments provide us with satisfactory answers to the research questions (Q1 and Q2) posed at the beginning of Section 2.4.

Specifically, adaptive force scaling controller utilizing $\tau_3 = \tau_a^{\mathrm{opt}}$ significantly outperformed those under τ_1, τ_2, τ_4, τ_5, and τ_6 in terms of F_H^{ave}, η, and P^{ave}. Hence, empirical evidence for an optimum admittance time constant was provided, which reinforce our theoretical analysis in Section 2.3.

Moreover, in terms of the gain profile, adaptive admittance gain used in C1 is more desirable than those suggested in the literature (C2 and C3). In particular, the proposed profile results in lower F_H^{ave} and P^{ave} and higher η than those calculated for C2 and C3. In addition, parking accuracy under C1 was better than that of C2, whereas C1 and C3 performed similarly, as anticipated. When the effort made by subjects to move the cart and parking accuracy are considered together, C1 outperformed C2 and C3.

Figure 2.11a shows the actual gain profile recorded for one subject under C1 during one of the experimental trials. It indeed follows a trend similar to the desired gain profile suggested in Section 2.2 (see Figure 2.2b). This shows that our approach successfully combines human intention and the different requirements of task phases as proposed in this study.

As shown in Fig 2.11a, the scaling gain increased from its nominal value till it reached its permissible upper limit during the driving phase, allowing maximum assistance to the subject for acceleration. Once a deceleration intention of the subject was detected, the gain gradually decreased to a minimum value (i.e., maximum attenuation), allowing the subject to decelerate the cart. As soon as the parking started, a high level of attenuation for the force was already reached, allowing the subject to park the cart more accurately.

Altering the gain in real-time can pose a threat in terms of stability if the instantaneous change in gain is too abrupt. There is a passivity approach suggested in the literature [63] to monitor the energy exchange during real-time pHRI. In Figure 2.12, we present the estimated energy exchange for all trials of one subject and also the average of all subjects under the proposed controller C1. This figure illustrates that the monitored energy never goes below zero in any of the trials, and hence the passivity is maintained.

Since we utilize adaptive gain controllers (C1, C2 and C3) which are time-varying, we can inspect the modes of the system to further investigate the stability [42]. Due to the time-varying nature, these modes cannot be extracted analytically. However, we can identify them from the collected experimental data by utilizing the model analysis methods suggested in [64, 65]. We performed such an analysis on the experimental data considering all the trials implemented by all subjects under C1, C2, and C3. Fig 2.13 shows the first eight modes of the coupled system under each controller (C1, C2, C3). As it can be observed, all modes under each controller are bounded, indicating that the system is uniformly stable [64, 66].

Finally, although there are no particular restrictions in applying the proposed approach to more realistic pHRI scenarios involving point-to-point manipulation of objects in 3D space, tuning in some parameters may be required depending on the task. In the future, we plan to work on a 3D co-manipulation task in which a user and robot lift a heavy object together and put it on a shelf. Our aim is to reduce the effort made by the user during the lifting by adjusting the force scaling gain on the fly using the proposed approach.

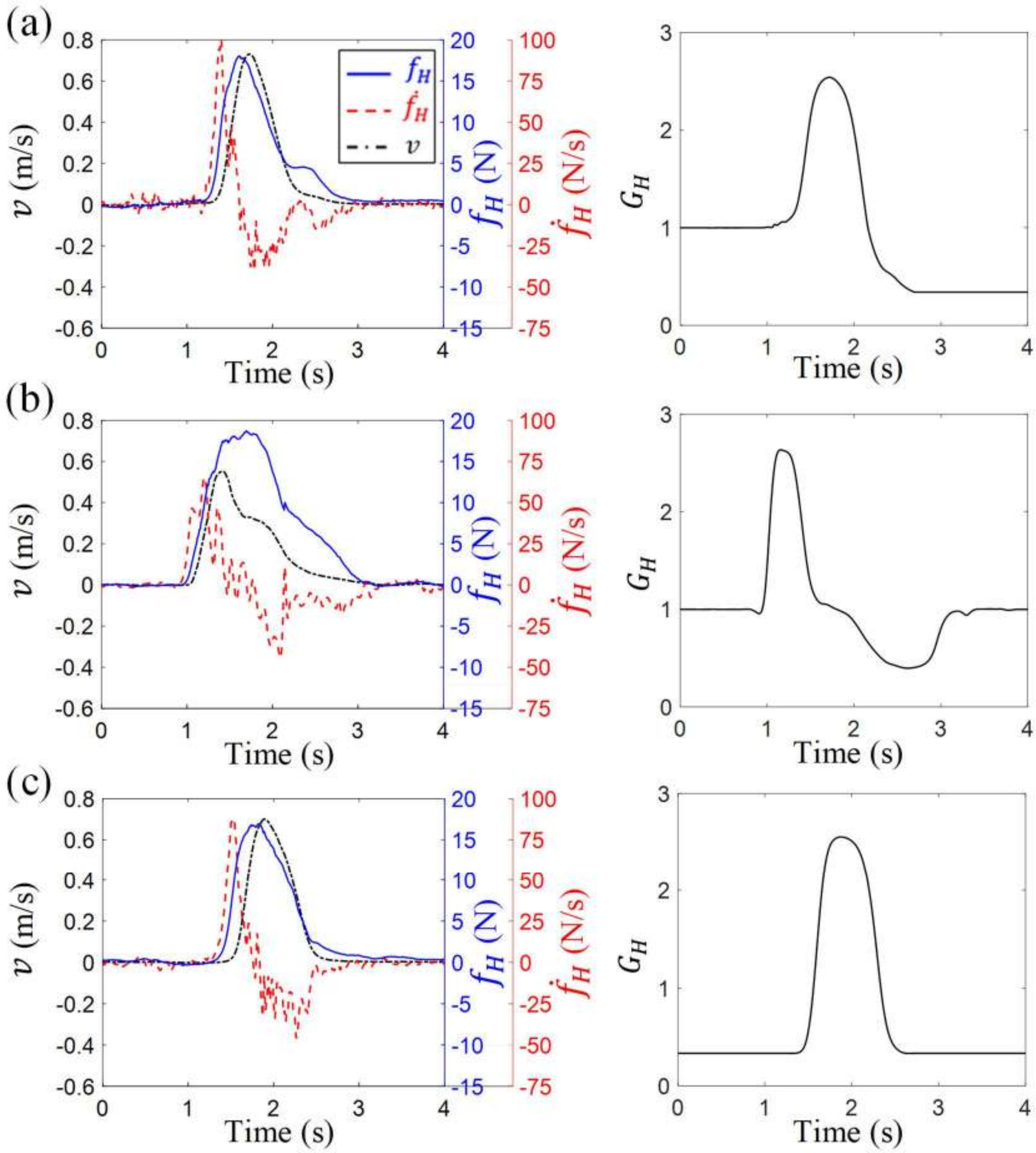

Figure 2.11: Cart velocity v, force applied by human f_H, its derivative $\dot{f}_H$, and adaptive gain G_H, as functions of time for exemplary trials of one subject under the controllers of a) C1 (our proposed controller), b) C2, and c) C3.

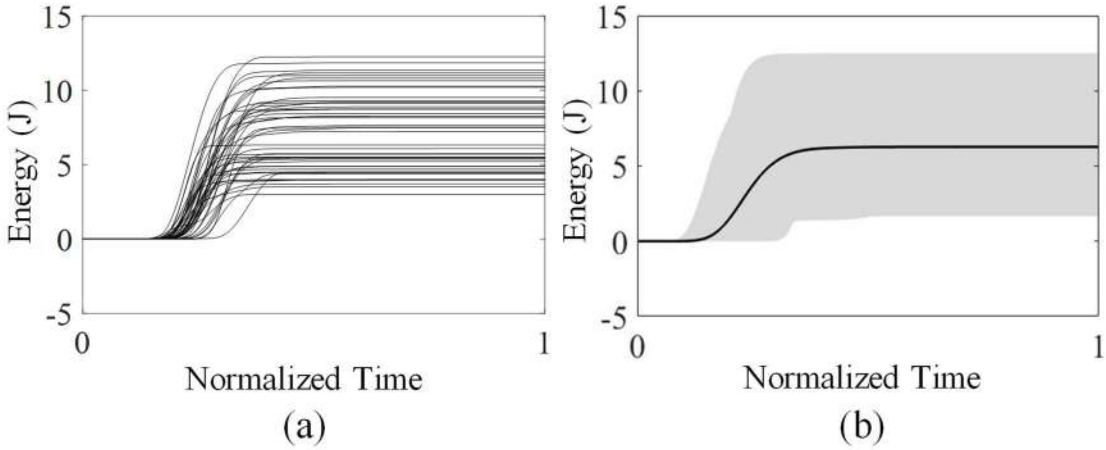

Figure 2.12: a) Energy exchange for one subject as a function of normalized time (solid curves represent the individual trials), b) Average energy exchange of all subjects (solid curve) under the proposed controller C1. The minimum and maximum energies of all trials for all subjects at each time step were utilized to construct the boundaries of the shaded region.

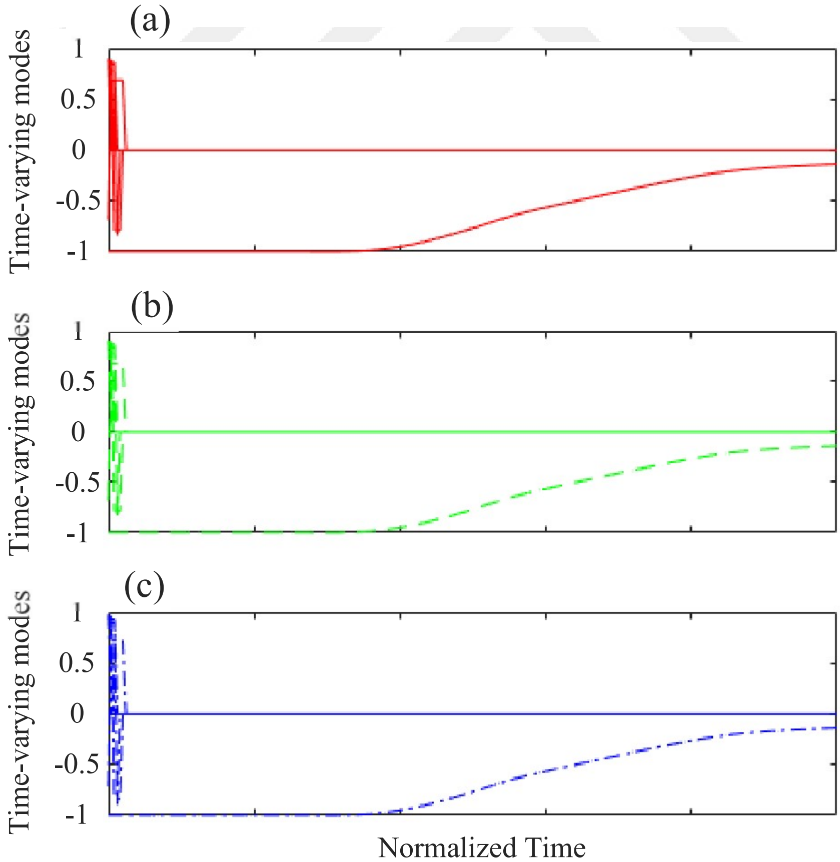

Figure 2.13: The modal analysis of the first eight modes of our pHRI system performed on the experimental data of all subjects under three different adaptive gain controllers; a) C1 (our proposed controller), b) C2, and c) C3.

Chapter 3

RESOLVING CONFLICTS DURING HUMAN-ROBOT CO-MANIPULATION

In this chapter, we aim at adjusting a robot's behavior to adaptively cooperate with a human while performing an object manipulation task. To achieve this, we propose an approach that enables the robot to detect the dyadic interaction behaviors emerge during the execution of the co-manipulation task. We utilize features derived from haptic data only as inputs to a machine learning algorithm to detect if both robot and human translate the object harmoniously or they face a conflict. Accordingly, a robot can lead the task proactively or act as a follower to a human partner in response to the detected interaction behaviors. For this purpose, we implement an admittance controller to regulate the interaction between human and robot, and an artificial potential field approach to define the trajectory for the proactive robot.

3.1 Approach

We focus on the dyadic interaction patterns that emerge during the collaboration between human and robot. We first detect those patterns using a ML algorithm and then adapt the response of the robot accordingly. In our pHRI scenario, human and robot cooperate to manipulate an object and transport it to a target location (see Figure 3.1). A flowchart representing our approach is shown in Figure 3.2. Initially, only the human knows the target location. Hence, the robot follows the movements of human partner initially based on the magnitude and direction of the forces applied by human. Once the direction of human force vector settles toward the intended target location, robot estimates it by intersecting the line in the direction of human force vector with a virtual boundary defined by the workspace of robot. Then, we utilize an artificial potential field (APF) approach to

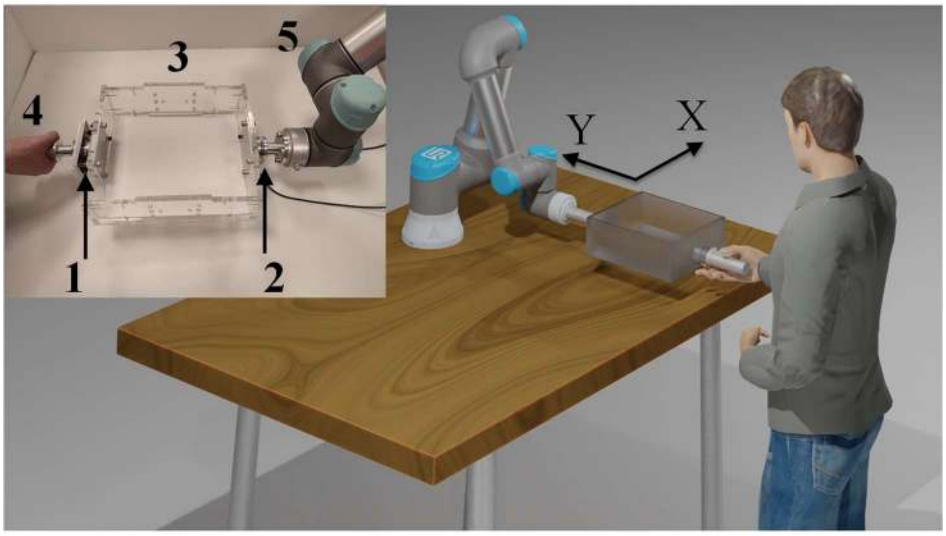

Figure 3.1: Human-robot co-manipulation scenario. Upper left figure shows the force sensors attached to the object for measuring the forces applied by human (1) and robot (2), the actual object being manipulated (3), human hand (4), and our collaborative robot (5).

generate a trajectory for robot towards the estimated target location. At this stage, robot is proactive and moves the manipulated object with the human partner toward the estimated target location. During this manipulation, if human changes the target location, a conflict arises. To detect these conflicts using ML, we rely on haptic-related features (derived from the forces/torques (i.e., wrenches) applied by the partners on the object) only. These features are fed to a ML model to detect three interaction patterns in our approach, which are:

1) **Working in harmony (WH):** The partners agree on the target direction; hence, they move the object harmoniously.
2) **Conflict in target direction (CD):** The partners face a conflict in movement direction since each aims a different target location.
3) **Conflict in parking location (CP):** The partners face a conflict in parking location since one of them aims to park the object before or after the target location.

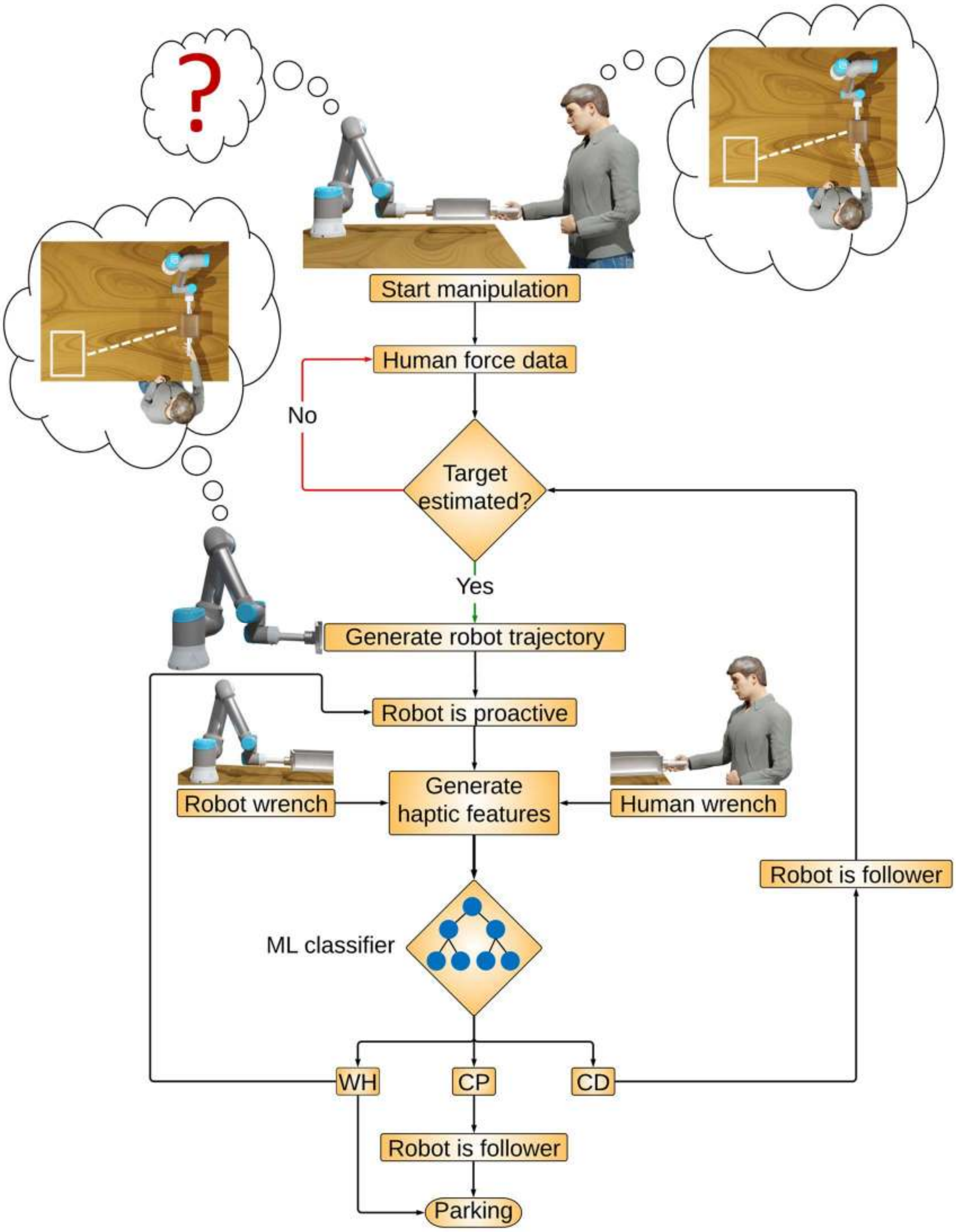

Figure 3.2: The flowchart of the proposed pHRI approach for co-manipulation of an object. WH, CP, and CD are working in harmony, conflict in parking location, and conflict in target location interaction behaviors, respectively. A random forest algorithm is used as the ML classifier in this study.

The ML classifier detects these behaviors and notifies the interaction controller of the robot to generate a suitable response. If WH pattern is detected, the controller maintains the proactive status of robot (see Figure 3.2). On the other hand, if CD is detected, the controller switches the robot status to a follower till a new target location is determined; hence a new trajectory is generated (see Figure 3.2). In CP, robot abandons its trajectory and acts as a follower to assist human in parking the object without facing a conflict. To avoid any jerky motion in CD and CP because of the switching between robot states, we gradually scale down the robot's attractive force to zero level once the robot turns from a proactive state to a passive state.

3.1.1 Hardware Setup

The setup used in our experiments, shown in Figure 3.1, consists of a collaborative robot (UR5, Universal Robot Inc.), a box-shaped object made of plexiglass with dimensions of 30 cm × 25 cm × 10 cm and having a weight of 2.5 kg, two force/torque (F/T) sensors (Mini45, ATI Inc.), and a computer screen to provide visual feedback for the subjects. Human and robot were jointly coupled through the manipulated object. One side of the object was rigidly connected to the robot through a force/torque sensor to measure the wrenches applied by robot. Human holds the object from the other side through an aluminum handle. A force/torque sensor was attached to this handle to measure the wrenches applied by human. All data was acquired at 125 Hz by an external DAQ card (USB-6343, National Instruments Inc.) connected to a personal computer.

3.1.2 Control Architecture

The control architecture utilized in this study is shown in Figure 3.3. An admittance controller is utilized to regulate the interactions between human and robot during the co-manipulation of object. Initially, the target location is unknown to robot, which starts the task as a follower to human. Hence, the ML classifier is not active, and only human force F_H is fed to the admittance controller to generate the reference velocity V_{REF} for the robot's motion controller, which in turn, transmits torques to robot joints to move the object with the velocity of V. Once the target location is estimated by the robot based on the direction of human force, a trajectory is generated for the robot using the APF and the robot is

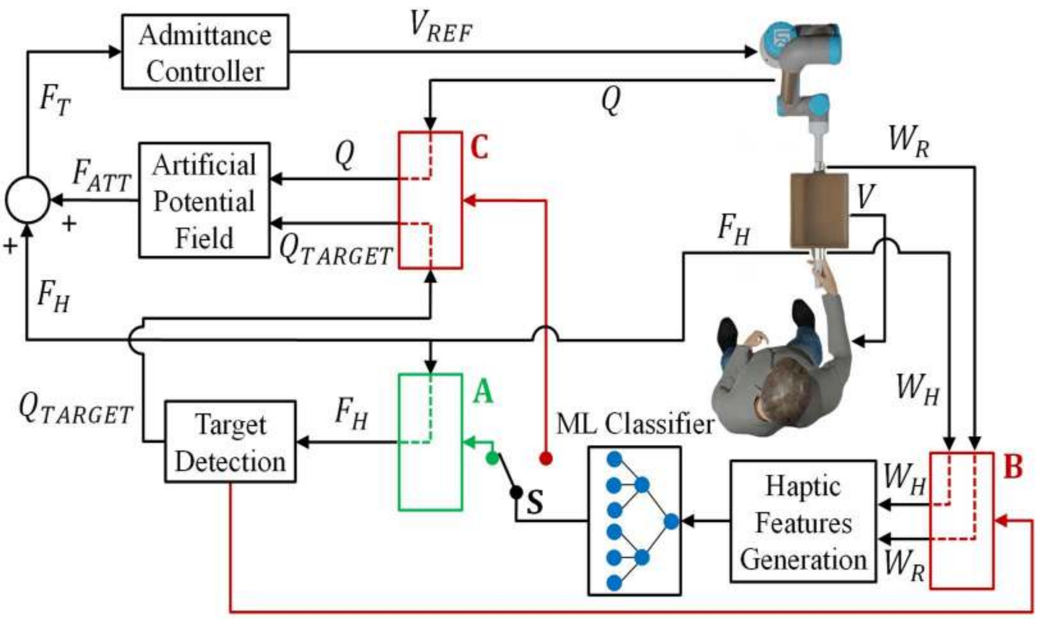

Figure 3.3: The control architecture utilized in our pHRI approach to regulate the harmonious and conflicting interactions between human and robot. A random forest algorithm is used as the ML classifier in this study.

pulled to the estimated target location with an attractive force F_{ATT} (we assume no obstacles in the environment, hence the repulsive force is zero). Here, the force applied by human partner F_H is added to F_{ATT} and the total force F_T is sent to the admittance controller. At this stage, ML classifier is active and utilizes the haptic-related features generated from the wrenches applied by human and robot to the object (W_H and W_R) to predict the interaction pattern. If WH is detected, the robot contributes to the task proactively. On the other hand, if a conflicting pattern (CD or CP) is detected, the controller switches the robot to a follower.

In Figure 3.3, blocks A, B, and C do not pass their corresponding data unless they are switched on via the logical command of their central input lines. Note that the two-way switch S normally turns on block A while deactivates Block C (i.e., robot is a follower), which is the starting phase of the motion in our approach. Then, if target location is determined, block B is activated; hence machine learning is involved. Consequently, switch S, which works based on the classifier decision, activates block C whenever WH pattern is detected. On the other hand, if the ML classifier observes one of the conflicting patterns (CD or CP), block C is deactivated by switch S, and the robot is a follower again.

Admittance Controller: The transfer function model of the admittance controller utilized in this study is:

$$Y(s) = \frac{V_{REF}(s)}{F_T(s)} = \frac{K_a}{\tau_a s + 1} \tag{3.1}$$

where, K_a and τ_a are the admittance gain and time constant, respectively, $V_{REF}(s)$ and $F_T(s)$ are the Laplace domain representations of the reference velocity and the total force, respectively.

3.1.3 Trajectory Generation

In this study, we utilize an APF approach to generate a trajectory for the robot so it can proactively cooperate with human partner. In APF, the total potential field, $U(Q)$, is made of attractive, $U_{ATT}(Q)$, and repulsive, $U_{REP}(Q)$, fields [67]. Then, the total force acting on the robot can be calculated by taking the negative gradient of the total potential field. In our approach, we assume that there are no physical obstacles in the environment and ignore the repulsive field (even if there are some obstacles, human can perceive the environment and she/he can direct the robot to avoid colliding with them). Hence, the attractive force acting on the robot is calculated by $F_{ATT} = -\nabla U_{ATT}$. The attractive force (the contribution of the robot to the task) starts at its maximum value and gradually reduces to zero as the target is reached.

To avoid high attractive forces far from the target, we utilize a hybrid APF that combines quadratic and conic formulas as follows [67]:

$$F_{ATT} = \left\{ \begin{array}{ll} -\xi(Q - Q_{TARGET}) & \text{if } \rho_{TARGET}(Q) \le d_t \\ -d_t\, \xi \dfrac{(Q - Q_{TARGET})}{\rho_{TARGET}(Q)} & \text{if } l - d_s > \rho_{TARGET}(Q) > d_t \\ -d_t\, \xi \dfrac{(Q - Q_{TARGET})}{\rho_{TARGET}(Q)}\, m & \text{if } \rho_{TARGET}(Q) \ge l - d_s \end{array} \right\} \tag{3.2}$$

where ξ, Q, Q_{TARGET}, d_t , $\rho_{TARGET}(Q)$, and m are positive constant scaling factor, current position vector, target position vector, a limit distance around the target for using the quadratic formula, the Euclidean distance to target $\|Q - Q_{TARGET}\|$, and the modification variable $\left(\left(d_s - \rho_{START}(Q)\right)/l\right) + \left(\rho_{START}(Q)\right)/d_s$, respectively.

Since the attractive force starts at its maximum value (i.e., $F_{ATT} = d_t\, \xi$) which causes a jerky motion at the beginning of the task, we slightly modified the original APF approach by introducing three new variables (see Figure 3.4); $l = \|Q_{START} - Q_{TARGET}\|$, $\rho_{START}(Q) = \|Q - Q_{START}\|$, and d_s is a limit distance around the starting point.

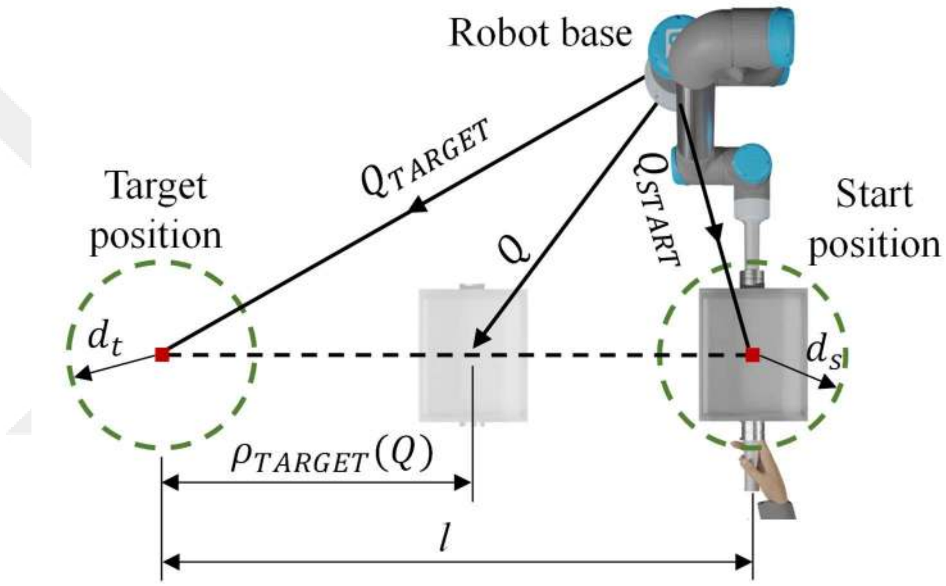

Figure 3.4: The parameters used for implementing the hybrid formulation for APF.

To implement the APF, the position of the target Q_{TARGET} should be known by the robot. However, estimating the intended target location at the very beginning of the movement, which is only known by human, is not trivial. In our approach, initially, robot has no prior information about the target location; hence it starts the task as a follower while human guides it toward the target by applying forces to the manipulated object. Once the direction of the human force vector settles toward a specific direction, robot utilizes this direction to estimate the target location by intersecting the vector of human force with a virtual task boundary within the robot workspace. For this purpose, we first measure the angle (θ) between the human force vector and the x-axis of robot. Then, we select a sliding buffer of size n for the measured data and compute the mean of the absolute differences between the angles in this buffer and their average. When this mean value is less than a specific threshold value (i.e., $(\sum_{i=1}^{n}|\theta_i - \theta_{AVE}|/n) < \theta_{THR}$), we consider that the human force vector settled in the desired direction without a considerable deviation. Note that when human changes the target location by altering the movement direction during the manipulation while robot is still active and moves toward the initial target, conflict in target direction (i.e., CD) emerges. Once robot detects this conflict, it leaves its own trajectory and follows the human passively till estimating the new target location and generating a new trajectory.

Finally, in our current implementation of APF, we assume that no rotational motion is involved, and the task is only performed to translate the object in the xy plane. Therefore, to estimate the target location, the intersection of the human force vector is taken with a virtual circle around the robot base representing the task boundary. However, we can easily extend the implementation of APF in 3D translational movement. In this case, if human intends to move the object to any location within the workspace, this location is estimated by the robot by intersecting human force vector with a virtual sphere around the robot base. Note that since we utilize UR5 robot in our experiments, the dimensions of that circle and the sphere are considered based on the practical dimensions of the UR5 robot workspace.

3.2 Experiments

In order to train and validate our ML classifier, we designed and implemented two sets of pHRI experiments:

1- **Training Experiments:** These experiments were designed to train and test the ML time-series classifier, relying on haptic features in distinguishing the interaction behaviors between human and robot partners.

2- **Validation Experiments:** These experiments were designed to investigate the potential benefits of the proposed ML approach in comparison to two other approaches.

All experiments utilized the same setup (see Figure 3.1), and the object manipulations were mainly involved translation and performed in the xy plane. The experimental study was approved by the Ethical Committee for Human Participants of our university. The values of the parameters used in the implementation were selected as; $K_a = 0.0167$, $\tau_a = 0.054$, $d_t = 8$ cm, $d_s = 4$ cm, $n = 30$, $\xi = 125$, and $\theta_{THR} = 0.08$ rad.

3.2.1 Training Experiments

3.2.1.1 Training Scenarios

The objective in designing the training scenarios is to collect haptic data to train a classifier model that can effectively distinguish between different interaction patterns (WH, CD, CP). To this end, 16 different manipulation scenarios, listed in Table 3.1, were introduced by covering as many different combinations of interaction behaviors as possible without being too exhaustive. In these training scenarios (TS), human and robot collaborate to move the object from the starting location to one of the target locations shown in Figure 3.5 (A, B, C, D, E, F). In designing these scenarios, we intentionally created harmonious and conflicting behaviors by assigning a specific target location for the robot and hence a trajectory to follow regardless of the human partner's target location. As a result, harmonious/conflicting interaction patterns resulted from the agreement/disagreement between the partners.

Table 3.1: Training scenarios and the expected interaction behaviors.

Training scenario (TS)	Robot target	Human target		Expected behavior
		Initial	Final	
TS1	B	B	B	WH
TS2	E	E	E	WH
TS3	B	E	E	CD
TS4	E	B	B	CD
TS5	B	A	A	WH, CP
TS6	B	C	C	WH, CP
TS7	E	D	D	WH, CP
TS8	E	F	F	WH, CP
TS9	B	B	F	WH, CD
TS10	E	E	B	WH, CD
TS11	E	B	D	CD, WH, CP
TS12	E	B	F	CD, WH, CP
TS13	B	E	A	CD, WH, CP
TS14	B	E	C	CD, WH, CP
TS15	E	B	E	CD, WH
TS16	B	E	B	CD, WH

To put things into context, consider training scenario 8 in Table 3.1, where both the human subject and the robot have the same target direction but different locations; therefore, they are expected to work in harmony (WH) initially to move the object toward that direction. However, as the human's scenario requires her/him to park the object (at target F in Figure 3.5) before the robot's target (target E in Figure 3.5), they face a conflict in parking location CP.

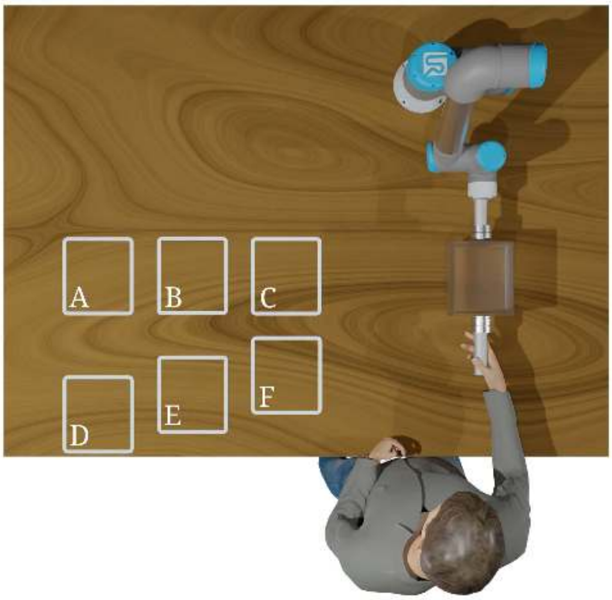

Figure 3.5: Scenarios used in training experiments.

3.2.1.2 Participants and Protocol

The training experiments were performed with 8 subjects (2 females and 6 males with an average age of 26.25 ± 4.2 SD). Prior to the experiment, subjects were instructed about the experimental procedure. They were not aware of the robot's target and explicitly instructed to move the object toward their own targets regardless of robot's behavior. Subjects performed the task by following the text instructions and visual images displayed on a computer monitor and the software sounds displayed during the experiment. In order to familiarize themselves with the setup, all subjects performed one manipulation trial involving harmonious collaboration (WH) with the robot. Thereafter, each subject performed the experimental scenarios listed in Table 3.1 in four separate sessions with 5 minutes break between the sessions. Each subject performed 32 trials, where each scenario repeated twice. The order of the scenarios was randomized in each session, while the order for all subjects was the same.

Subjects started the experiment by handling the object from one side while facing the robot handling the object from the other side by its end effector. To provide visual feedback to the subjects, the initial and target locations were displayed as static 2D rectangles in white color while the current location of the manipulated object was displayed as a moving 2D rectangle in pink color through a computer screen. A text message on the computer screen along with a distinct software sound were used to start the task. During the execution of task, if the scenario involved a change in target location, the new target location was updated immediately on the computer screen to notify the subject. When the subject reached the target location, the color of the rectangle at the target changed to green to notify the subject, and after staying at the target location for 2 seconds, a message appeared on the screen along with a distinct beep notifying the subject to park the object.

3.2.1.3 Haptic Features and Classifier Design

The raw haptic data (i.e., wrenches applied by human and robot) collected during the training experiments are annotated and segmented based on the expected behaviors listed in Table 3.1 by following the procedure employed in [49]. As demonstrated in this work, the features extracted from the haptic data alone are sufficient to distinguish between different interaction patterns. We utilize the haptic features, originally suggested by Noohi and Žefran [68] and extended by Al-Saadi et al. [49] to train our ML classifier. We briefly mention them here for the sake of discussion, but the details are available in [49],[68].

Consider Figure 3.6, where F_H, F_R , and F_{SUM} are the forces applied on an object by human, robot, and their summation, respectively. That is:

$$F_{SUM}(t) = F_H(t) + F_R(t) \tag{3.3}$$

The effective forces of human F_H^* and robot F_R^* that contribute to the task are calculated as the projection of their forces on F_{SUM}.

$$F_H^*(t) = \mu\, F_{SUM}(t) \tag{3.4}$$

$$F_R^*(t) = \beta\, F_{SUM}(t) \tag{3.5}$$

where t is the time step and $\mu + \beta = 1$. On the other hand, the forces that are perpendicular to F_{SUM} (i.e., F_{NORMAL} in Figure 3.6) do not contribute to the task and are canceled by each other.

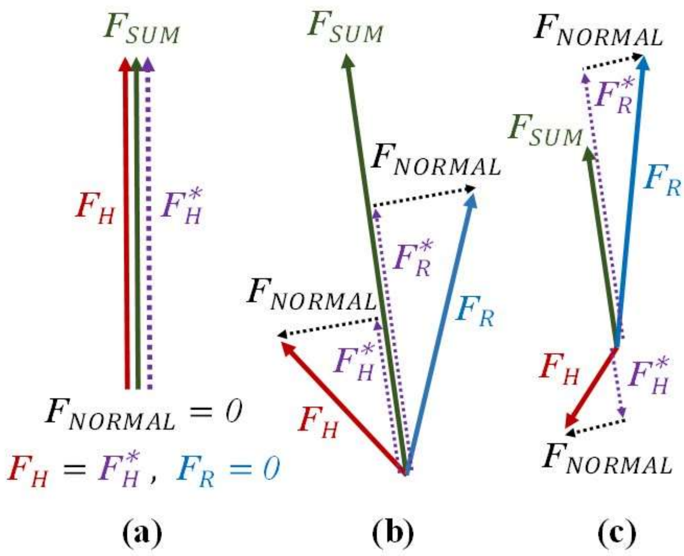

Figure 3.6: Force decomposition. F_H, F_R, F_H^*, F_R^*, F_{NORMAL} and F_{SUM} stand for human applied force, robot applied force, human effective force, robot effective force, normal force, and summation of human and robot forces, respectively.

Based on this force decomposition, five force-related features were introduced, namely, individual force efficiency of human $M_{E_H}^F$, individual force efficiency of robot $M_{E_R}^F$, team force efficiency M_{TE}^F, negotiation force efficiency M_{NE}^F, and similarity of forces M_S^F. Moreover, since this decomposition was extended in [49] by including the torques applied by human (T_H) and robot (T_R), five additional torque-related features were introduced: individual torque efficiency of human $M_{E_H}^T$, individual torque efficiency of robot $M_{E_R}^T$, team torque efficiency M_{TE}^T, negotiation torque efficiency M_{NE}^T, and similarity of torques M_S^T. Note that the superscripts F and T refer to force and torque-related features, respectively. For more information about these metrics, please refer to [49].

The study in [49] showed that analyzing the task in different movement planes resulted in more informative features than analyzing it in 6-dof space. For that, we performed the force/torque decomposition in the three principal movement planes, xy, xz, and yz. This ended up with 30 wrench-related features (10 wrench-related features × 3 planes) that were inputted into our classifier. We utilized a random forest algorithm to train our time-series classifier model to discriminate between the interaction patterns. Random forest is a supervised learning algorithm used for both regression and classification. In classification, it constructs a multitude of decision trees and outputs the class selected by most of them. Python Scikit-Learn package was utilized for the implementation of the algorithm [69]. The number of trees in the random forest was set to 100 while the maximum depth of the trees was unconstrained.

We split the dataset into two distinct sets: training and test. To train (test) the classification model, we used the data coming from 24 (8) trials of each subject. Since there were 8 subjects, the total number of trials for training and testing were 192 (75%) and 64 (25%), respectively. We achieved a classification accuracy of 88.82% and a BER of 0.11 after cross-validation. Figure 3.7 shows the confusion matrix for the classifier.

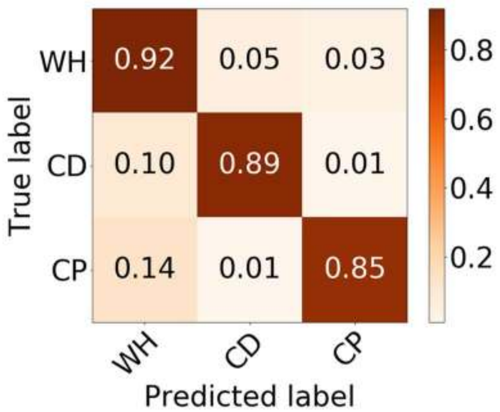

Figure 3.7: Confusion matrix for classifier trained with haptic feature set. WH, CD, and CP stand for working in harmony, conflict in target direction, and conflict in parking location behaviors, respectively.

3.2.2 Validation Experiments

To evaluate the performance of our proposed approach, we implemented another set of experiments utilizing the same setup and scenarios. Recalling the co-manipulation example discussed in the introduction section, where robot acts either as a follower or interacts proactively with human, we considered 3 experimental conditions (EC1, EC2, and EC3). The first condition, EC1, implements a simple leader-follower model where the robot is passive and always follows human. In EC2, robot has a fixed target location, and hence it follows a trajectory based on the APF method, regardless of the agreement/disagreement with human partner. In this condition (EC2), robot assists the human partner (i.e., contributes to the task) if they have the same target. Nevertheless, when they are given different target locations, they display conflicting behavior, which cannot be resolved. Finally, the EC3 condition utilizes our proposed approach of integrating the APF method with the ML classifier for conflict resolution.

Three different experimental scenarios (ES1, ES2, and ES3) were considered for the validation experiments (Figure 3.8). In ES1, human and robot work in harmony (WH) to transport the object to a target position (point B), while in ES2, the target location changes suddenly from location B to location E, causing a conflict in movement direction (CD). Finally, in ES3, the target location suddenly changes from location B to location C, causing a conflict in parking location (CP).

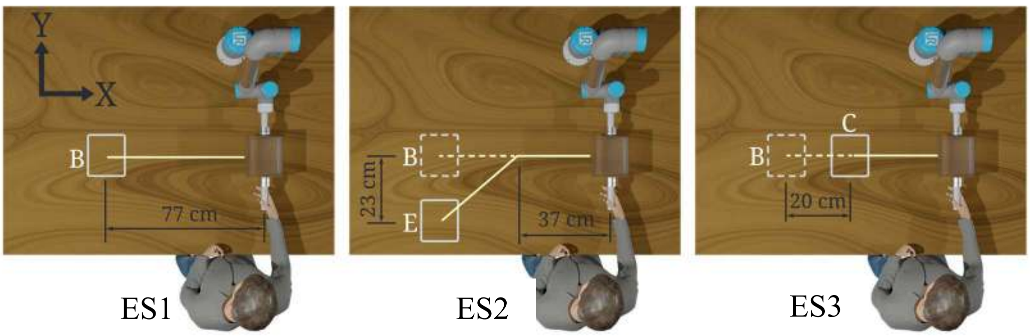

Figure 3.8: Experimental scenarios (ES) used in validation experiments.

Six subjects, with an average age of 25.5 ± 4.4 SD, participated in this experiment. Each experimental condition (EC1, EC2, and EC3) was repeated twice for each experimental scenario (ES1, ES2, and ES3). Hence, the total number of trials performed by each subject was 18, which were completed in two sessions with 5 minutes break between the sessions. The order of the experimental conditions and scenarios was randomized in each session while the same order was displayed to each participant.

3.2.2.1 Results and Discussions

3.2.2.1.1 Force Profiles and Classifier Performance

Figure 3.9 represents the force profiles of a representative dyad (a subject and robot) for ES1, ES2, and ES3 under EC3 (our approach) in tandem with the decisions taken by the classifier. We concentrated on the forces applied in xy plane, which is the plane of most movements in our experiment. In all plots, subscripts H and R stand for human and robot, respectively. The blue and red lines in Figure 3.9a represent the forces applied by human and robot, respectively (please note that all forces were presented with respect to the manipulated object frame), while Figure 3.9b depicts the raw predictions RP (green line) and processed predictions PP (orange transparent line) of the ML classifier. As shown in Figure 3.9b, the classifier successfully predicted the interaction behaviors in all experimental scenarios. Moreover, the classifier was able to predict the conflicting behaviors (i.e., CD in ES2 and CP in ES3), which occurred for short periods of time only, and instructed the controller to resolve the conflicts by switching the robot to a follower state. Prior to sending the classifier decision to the controller, a voting buffer was implemented:

Voting buffer. This buffer holds the raw predictions for the previous time steps and outputs the most frequent prediction. The length of this buffer is 20 samples, with an overlap of 10 samples between each buffer. Using this buffer eliminates the instantaneous misclassifications due to the sudden and unintentional movements of the subjects. For instance, although some patterns were misclassified initially (i.e., a CP in ES2 and some CDs in ES1 in Figure 9b), they were filtered out by the voting buffer.

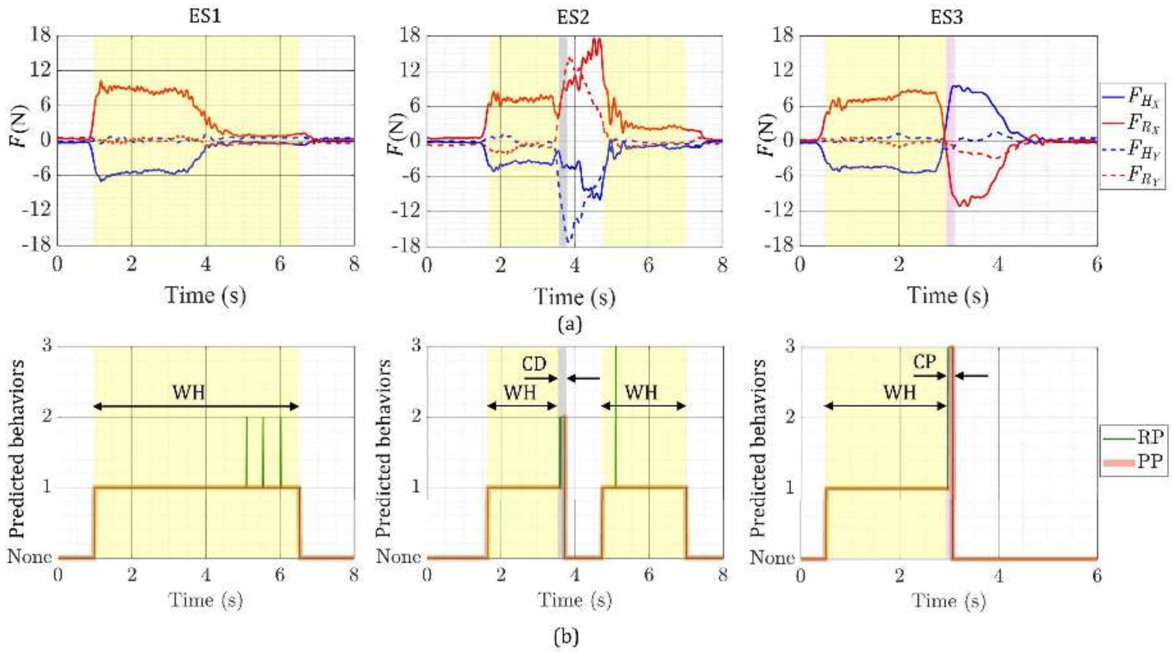

Figure 3.9: (a) Forces profiles of a human subject (blue) and robot (red), and (b) the raw predictions (RP) by ML and the processed predictions (PP) after filtering for the experimental scenarios ES1, ES2, and ES3 under our proposed approach (EC3). Subscripts H and R stand for human, robot, respectively. The predicted values 1, 2, and 3 stand for WH, CD, and CP interaction behaviors, respectively, while "None" stands for the periods where ML is inactive, and the robot is follower.

By inspecting the interaction behaviors in Figure 3.9, we observed that they produced highly complex force profiles though the object manipulations were translational (no rotations) and mainly performed in xy plane. For example, the yellow-colored shaded areas in Figure 3.9 correspond to WH behavior, in which the partners harmoniously translated the object toward the target. One anticipates that partners perform the manipulation by exerting forces in the same direction of the movement during this type of interaction. However, when the force profiles in Figure 3.9a are inspected carefully, one observes that only human partner applies forces in the direction of the movement while the forces applied by robot are in the opposite direction. The reason for this mismatch is due to the delay in the reaction times of the partners to each other's actions as also observed in human dyads [49].

The grey-colored shaded area in Figure 3.9 corresponds to CD behavior, in which the partners disagreed on the target direction. This behavior occurred in ES2 scenario: a new target location (location E in Figure 3.8) was suddenly displayed to the subject, and he started to apply forces in the negative y-axis to move the object toward the new target location. On the other hand, as the robot was still actively moving toward the original target location (location B in Figure 3.8), it resisted human movement, which resulted in the opposing forces applied by the partners along the y-axis. By inspecting the force patterns during this behavior, we observed that they changed in both x and y directions, although the new target position deviated from the initial one along the y-direction only.

Finally, in CP behavior (the pink-colored shaded area in Figure 3.9), the subject and robot had given the same target location of B as shown in ES3 in Figure 3.9, but the subject was instructed later to park the object suddenly at location C prior to the target location B. Subject applied forces opposite to the direction of movement (along x-axis) to park the object at location C, as clearly shown in Figure 3.9a for ES3 (see the change in the direction of forces in the pink-colored shaded region). However, since the robot was moving the object toward the original target location B, it applied forces opposite to the direction of forces applied by the subject.

3.2.2.1.2 Task Performance Under EC1, EC2, and EC3

We used the following metrics [51] [70] to evaluate the task performance of the subjects: the average velocity of the object ($V^{\mathrm{AVE}} = 1/(t_f - t_i)\int_{t_i}^{t_f} |V(t)|\, dt$), average force applied by subject ($F_H^{\mathrm{AVE}} = 1/(t_f - t_i)\int_{t_i}^{t_f} |F_H(t)|\, dt$), average power consumed by subject ($P^{\mathrm{AVE}} = 1/(t_f - t_i)\int_{t_i}^{t_f} |F_H(t).V(t)|\, dt$), and the task completion time (TCT). Here, t_i and t_f are the time when the object velocity just exceeded 2% of the maximal velocity and the ending time of the trial, respectively. TCT was computed by measuring the time starting from t_i till completing the trial.

Figure 3.10 presents the mean and standard error of means of the performance metrics of the subjects under each experimental condition (EC1, EC2, and EC3) for each scenario. We performed a one-way ANOVA with Tukey post-hoc test to examine the effects of the experimental conditions on the performance metrics.

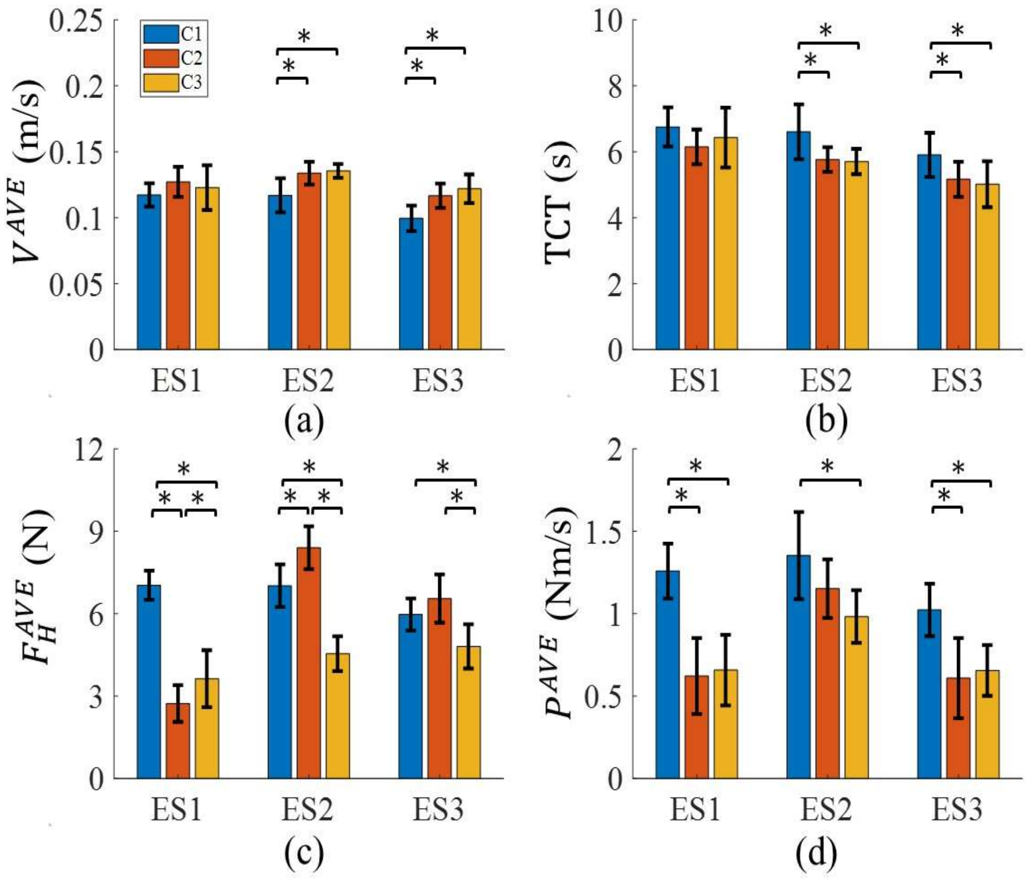

Figure 3.10: Mean values of the performance metrics for three experimental scenarios ES1, ES2, and ES3 under three different experimental conditions EC1, EC2, and EC3. Error bars are the standard deviations of means and horizontal bracket with * on top indicates statistically significance pairwise comparisons with $p = 0.05$.

Figure 3.10a (3.10b) shows that V^{AVE} (TCT) under EC2 and EC3 were significantly higher (lower) than that of EC1 in both ES2 and ES3. Although, V^{AVE} (TCT) under EC2 and EC3 were higher (lower) than that of EC1 in ES1, the difference was not statistically significant. In addition, the differences in V^{AVE} and TCT between EC2 and EC3 were not significant in all experimental scenarios.

Figure 3.10c shows that the average forces applied by subjects F_H^{AVE} under EC3 (our proposed approach) were significantly lower than those of EC1 and EC2 in both ES2 and ES3, and lower than that of EC1 in ES1. In addition, F_H^{AVE} under EC2 was lower than those of EC1 and EC3 in ES1. This shows that the ML classifier in our proposed approach

(EC3) successfully resolved the conflicts between human and robot, and hence reduced the forces exerted by human to change the direction of movement or parking location. Additionally, the average forces applied by subjects F_H^{AVE} under EC2 were higher than those of EC1 in both ES2 and ES3. Although the APF utilized in EC2 reduced the task completion time compared to EC1, it caused the subjects to exert more force during the conflicting scenarios in ES2 and ES3.

In Figure 3.10d, we observe that subjects spent less effort P^{AVE} under EC2 and EC3 compared to that under EC1 due to the benefit of utilizing APF, especially in ES1. Moreover, when the conflict was stronger, as in ES2, EC3 led to less effort than that of EC2, thanks to our ML model in resolving the conflict. The results on P^{AVE} showed that the conflicts in parking (ES3) were more easily (with less effort) resolved than the conflicts in changing direction (ES2).

In summary, our proposed approach EC3 resolved the conflicts between the partners effectively, allowing subjects to exert less force than those under EC1 and EC2. However, in ES1, where no conflict happened, we can see that F_H^{AVE} under EC3 was higher than that of EC2. This is because the robot in EC2 was active through the whole task, while in EC3, human needs to apply forces to guide the robot as it starts the task as a follower. Although subjects applied less force under EC3, they translated the object with higher velocities and lower TCT (particularly compared to those under EC1). The results of the experiments show that our approach (EC3) reduces the average force applied by subjects by 42.65% and 30.6% compared to those under EC1 and EC2, respectively. Moreover, the average power spent by the subjects under EC3 was reduced by 46.27% and 4.94% compared to those of EC1 and EC2, respectively.

Finally, in any pHRI task, the stability of the interaction should be guaranteed to implement the task safely without endangering the human partner. Therefore, we utilized the passivity approach proposed in [63] to monitor the energy exchange during the manipulation task. Figure 3.11 shows the estimated energy exchange for all trials of all subjects under EC1, EC2, and EC3, and the average of the energies of all subjects. Figure 3.11 states that the energies in all trials do not go below zero; hence, the passivity of the pHRI interaction is not violated.

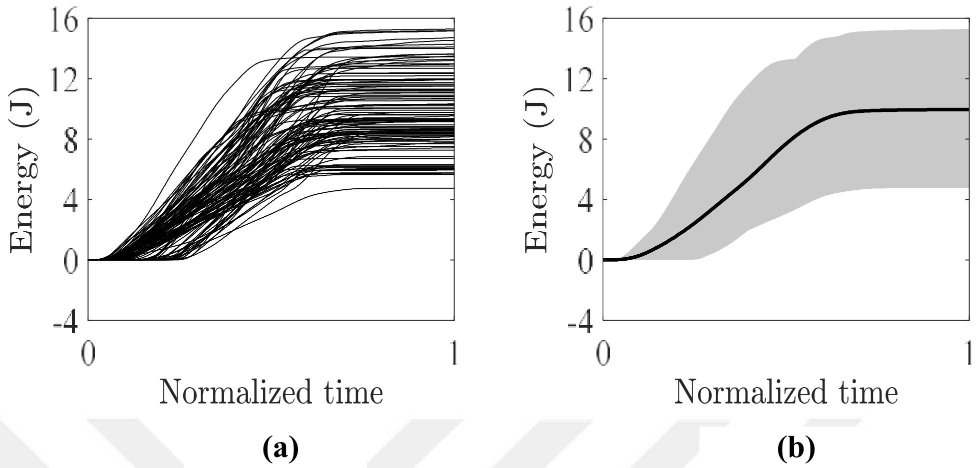

Figure 3.11: (a) Energy exchange for all subject as a function of normalized time (solid curves represent the individual trials), (b) Average energy exchange of all subjects (solid curve) under EC1, EC2, and EC3. The minimum and maximum energies of all trials for all subjects at each time step were utilized to construct the boundaries of the shaded region.

Chapter 4

CONCLUSION

In the first part of this dissertation, we proposed an approach for adaptive scaling of human force based on predicted human intention to achieve more effective co-manipulation in terms of task performance during pHRI. The proposed approach interprets human intention as to accelerate and decelerate the manipulated object while paying attention to the different phases of pHRI task. Human intention was quantified by a numerical value, which was then used to adapt the gain of an admittance controller without affecting its time constant. The results of the first set of experiments provided evidence to the existence of an optimum admittance time constant for a given co-transportation task. Moreover, the results of the second set of experiments suggested that the proposed profile for gain adaptation is superior to the ones proposed in the literature for the same purpose. In addition, the linear relation obtained between the movement time MT and the index of difficulty ID in both experiments suggested that Fitts's law is also valid for a pHRI task involving co-transportation of an object.

We verified our approach by implementing experiments to translate the object only in a single direction (i.e., x-axis). Although there are no particular restrictions in applying the proposed approach to more realistic pHRI scenarios involving point-to-point manipulation of objects in 3D space, tuning in some parameters may be required depending on the task. Also, involving rotational movements was not considered in the approach. Therefore, In the future, we plan to enhance our approach to work on a 6D co-manipulation task in which a user and robot lift a heavy object together and put it on a shelf. Moreover, the current approach is designed to manipulate an object in free space without involving direct contact with stiff environment. In the future, we aim to modify and test our approach in more realistic pHRI scenarios involving contact interactions with an environment to further demonstrate its potential in industrial applications [53][71]. Instead of using a rail system, virtual fixtures can be utilized to constrain the movements of manipulated object in those scenarios.

In the second part of this dissertation, we proposed an approach that allows the robot to proactively interact with a human partner based on the time-series classification of the interaction behaviors that arise while executing a collaborative task. During these interactions, conflicts may naturally arise if the partners have different movement intentions. To resolve these conflicts, we argue that it is important to study the dyadic interaction behaviors rather than the individual behavior of human partner. Moreover, we show that the haptic features derived from forces and torques alone are sufficient to detect these conflicts. In our approach, these features were inputted to a ML algorithm to train a classifier model that differentiates between the interaction patterns.

In order to demonstrate our approach, we designed a pHRI experiment where both human and robot collaborated to manipulate an object. Experimental scenarios that involve partners work in harmony and conflict with each other in movement direction and parking location were designed to test the efficacy of the proposed approach. The results showed that our ML classifier successfully recognized the interaction behaviors that emerged during those scenarios and instructed the robot to take proper action accordingly. Hence, the robot was able to adapt its behavior to act as a follower when there was a conflict or contribute to the task proactively when the dyad was working in harmony. As a result, the conflicts between human and robot during the manipulation were accommodated effectively and the subjects performed the task with lower effort.

Our current experimental scenarios involved translational manipulations of an object in 2D space. As a future work, we aim to extend our approach to more complex scenarios involving object manipulations in 6D space. In particular, we would like to show that a rule-based approach (e.g., defining some rules based on force magnitudes/thresholds) cannot successfully detect conflicts in such complex manipulation scenarios, or the same rules cannot be applied easily to other manipulation scenarios involving different sub-tasks or objects having different shape, weights or material properties (e.g., elastic objects). Additionally, we would like to design a questionnaire, similar to that done in [72], to measure the personal opinion of human subjects participating in our experiments about their sense of interaction with the robot under different experimental conditions and experimental scenarios. In particular, we are interested in quantifying the degree of conflict that they subjectively feel under those cases and how much of our current or future approaches help them to solve them.

Finally, both approaches proposed in this dissertation aim at improving the overall performance of the physical interaction between human and robot in an object co-manipulation task. Both approaches utilize admittance control to regulate the interaction between the partners. While the first approach relies on haptic data and velocity of an object to estimate human intentions to adaptively adjust the contribution of the robot to the task, the second approach relies on haptic data only to detect the dyadic intentions of both human and a proactive robot by defining the interaction behaviors between them and adjust the role of the robot accordingly. In the future, we aim to combine both approaches to further improve the performance of the pHRI task. For instance, while the ML classifier detects harmonious behavior between human and robot partners, utilizing adaptive admittance control by scaling human force based on the estimation of human movement intentions (i.e., acceleration or deceleration intentions) will intuitively reduce human effort and task duration. Moreover, when the ML classifier detects conflict in parking behavior, we can gradually scale down human forces to increase the parking accuracy.

BIBLIOGRAPHY

[1] J. Kruger, T. K. Lien, and A. Verl, "Cooperation of human and machines in assembly lines," in *CIRP Annals Manufacturing Technology*, vol. 58, no. 2, pp. 628–646, 2009.

[2] S. Y. Lee, K. Y. Lee, S. H. Lee, J. W. Kim, and C. S. Han, "Human–robot cooperation control for installing heavy construction materials," *Autonomous Robots*, vol. 22, pp. 305–319, 2007.

[3] S. Lee and J. Il Moon, "Introduction of human-robot cooperation technology at construction sites," in *International Symposium on Automation and Robotics in Construction and Mining (ISAR)*, vol. 31, pp. 1–6, 2014.

[4] J. Ernesto Solanes, Luis Gracia, Pau Muñoz-Benavent, Jaime Valls Miro, Marc G. Carmichael, and Josep Tornero, "Human–robot collaboration for safe object transportation using force feedback," *Robotics and Autonomous Systems*, 107, pp. 196–208, 2018.

[5] F. Semeraro, A. Griffiths, and A. Cangelosi, "Human-robot collaboration and machine learning: a systematic review of recent research," *arXiv:2110.07448v4*, 2022.

[6] A. Ajoudani, A. M. Zanchettin, S. Ivaldi, A. Albu-Schäffer, K. Kosuge, and O. Khatib, "Progress and prospects of the human–robot collaboration," *Autonomous Robots*, vol. 42, pp. 957–975, 2018.

[7] J. Han, S. Lee, and J. Kim, "Behavior hierarchy-based affordance map for recognition of human intention and its application to human–robot interaction," *IEEE Trans. Human–Mach. Syst.*, vol. 46, no. 5, pp. 708–722, 2016.

[8] A. Kucukyilmaz, T. Sezgin, and C. Basdogan, "Intention recognition for dynamic role exchange in haptic collaboration," *IEEE Trans. Haptics*, vol. 6, no. 1, pp. 58–68, 2013.

[9] H. Kazerooni and S. Mahoney, "Force augmentation in human-robot interaction," in *Proceedings of the 1990 American Control Conference*, vol. 3, pp. 2821–2826, 1990.

[10] N. Abroug, X. Lamy, and E. Laroche, "Human force augmentation: optimal control parameters tuning using structured H∞ synthesis," in *IEEE Int. Conf. Intelligent Robots and Systems*, pp. 702–709, 2016.

[11] B. Cagneau, G. Morel, D. Bellot, N. Zemiti, and G. d'Agostino, "A passive force amplifier," in *IEEE International Conference on Robotics and Automation (ICRA)*, pp. 2079–2084, 2008.

[12] F. Babel, J. M. Kraus, and M. Baumann, "Development and Testing of Psychological Conflict Resolution Strategies for Assertive Robots to Resolve Human-Robot Goal Conflict," *Front Robot AI*, vol. 7, article 591448, 2021.

[13] R. Ikeura, T. Moriguchi, and K. Mizutani, "Optimal variable impedance control for a robot and its application to lifting an object with a human," in *IEEE International Workshop on Robot and Human Interactive Communication*, pp. 500–505, 2002.

[14] G. Kang, H. S. Oh, J. K. Seo, U. Kim, and H. R. Choi, "Variable admittance control of robot manipulators based on human intention," in *IEEE/ASME Trans. Mechatronics*, vol. 24, no. 3, pp. 1023–1032, 2019.

[15] T. Tsumugiwa, R. Yokogawa, K. Hara, "Variable impedance control based on estimation of human arm stiffness for human-robot cooperative calligraphic task," in *IEEE Int. Conf. Robot. Autom.*, pp. 644–650, 2002.

[16] M. Rahman, R. Ikeura and K. Mizutani, "Investigating the impedance characteristics of human arm for development of robots to cooperate with human operators," in *IEEE Int. Conf. on Systems, Man and Cybernetics*, pp. 676–681, 1999.

[17] L. Peternel, N. Tsagarakis, and A. Ajoudani, "A human-robot co-manipulation approach based on human sensorimotor information," *IEEE Transactions on Neural Systems and Rehabilitation Engineering*, 25(7), pp. 811–822, 2017.

[18] S. Grafakos, F. Dimeas, and N. Aspragathos, "Variable admittance control in pHRI using EMG-based arm muscles co-activation," *in IEEE International Conference on Systems, Man, and Cybernetics (SMC)*, pp. 1900-1905, Oct 2016.

[19] A. Keemink, R. Fierkens, J. Lobo-Prat, J. Schorsch, D. Abbink, J. Smeets, and A. Stienen, "Using position dependent damping forces around reaching targets for transporting heavy objects: A Fitts' law approach," in *Biomedical Robotics and Biomechatronics (BioRob), 6th IEEE International Conference*, pp. 1323–1329, 2016.

[20] H.-Y. Li, I. Paranawithana, L. Yang, T.S.K. Lim, S. Foong, F.C. Ng, U.-X. Tan, "Stable and compliant motion of physical human robot interaction coupled with a moving environment using variable admittance and adaptive control," *IEEE Robotics and Automation Letters*, vol. 3, no. 3, pp. 2493–2500, 2018.

[21] H.-Y. Li., T. Nuradha, S. A. Xavier, U-X. Tan, "Towards a compliant and accurate cooperative micromanipulator using variable admittance control," in *IEEE 3rd International Conference on Advanced Robotics and Mechatronics (ICARM)*, pp. 230–235, 2018.

[22] T. Wojtara, M. Uchihara, H. Murayama, S. Shimoda, S. Sakai, H. Fujimoto, and H. Kimura, "Human-robot collaboration in precise positioning of a three-dimensional object," *Automatica*, vol. 45, no. 2, pp. 333–342, 2009.

[23] V. Duchaine and C. M. Gosselin, "General model of human-robot cooperation using a novel velocity based variable impedance control," in *Proceedings of the Joint EuroHaptics Conference and Symposium*, pp. 446–451, 2007.

[24] V. Duchaine, B. Mayer-St-Onge, D. Gao, and C. Gosselin, "Stable and intuitive control of an intelligent assist device," *IEEE Trans. Haptics*, vol. 5, no. 2, pp. 1939–1412, 2012.

[25] Y. Aydin, N. Arghavani, and C. Basdogan, "A new control architecture for physical human-robot interaction based on haptic communication," in *ACM/IEEE International Conference on Human- Robot Interaction*, pp. 122–123, 2014.

[26] A. Lecours, B. Mayer-St-Onge, and C. Gosselin, "Variable admittance control of a four-degree-of-freedom intelligent assist device," in *IEEE International Conference on Robotics and Automation*, pp. 3903–3908, 2012.

[27] F. Dimeas and N. Aspragathos, "Fuzzy learning variable admittance control for human-robot cooperation," in *IEEE International Conference on Intelligent Robots and Systems*, pp. 4770–4775, 2014.

[28] P. D. Labrecque, C. Gosselin, "Variable admittance for pHRI: from intuitive unilateral interaction to optimal bilateral force amplification," *Robot. Comput. Integr. Manuf.*, 52, pp. 1–8, 2018.

[29] X. Lamy, F. Colledani, F. Geffard, Y. Measson, and G. Morel, "Human force amplification with industrial robot: study of dynamic limitations," in *IEEE/RSJ International Conference on Intelligent Robots and Systems*, pp. 2487–2494, 2010.

[30] K. Kosuge, Y. Fujisawa, and T. Fukuda, “Control of robot directly maneuvered by operator,” in *Proceedings of the IEEE/RSJ International Conference on Intelligent Robots and Systems*, vol. 1, pp. 49–54, 1993.

[31] C. Luna, M. Rahman, M. Saad, P. Archambault, and S. Ferrer, “Admittance-based upper limb robotic active and active-assistive movements,” *Int. J. Adv. Robot. Syst.*, vol. 12, no. 9, pp. 117-130, 2015.

[32] L. M. Miller and J. Rosen, “Comparison of multi-sensor admittance control in joint space and task space for a seven degree of freedom upper limb exoskeleton,” *IEEE/RAS-EMBS International Conference on Biomedical Robotics and Biomechatronics*, pp. 70-75, 2010.

[33] R. Goljat, J. Babic, T. Petric, L. Peternel, and J. Morimoto, “Power-augmentation control approach for arm exoskeleton based on human muscular manipulability,” in *IEEE International Conference on Robotics and Automation (ICRA)*, pp. 5929–5934, 2017.

[34] S. O. Oguz, A. Kucukyilmaz, T. M. Sezgin, and C. Basdogan, “Supporting Negotiation Behavior with Haptics-Enabled Human-Computer Interfaces,” In *IEEE Transactions on Haptics*, vol. 5, no. 3, pp. 274-284, 2012.

[35] A. Mörtl, M. Lawitzky, A. Kucukyilmaz, M. Sezgin, C. Basdogan, and S. Hirche, “The role of roles: physical cooperation between humans and robots,” *The International Journal of Robotics Research,* 31(13), pp. 1656–1674, 2012.

[36] Mahdi Khoramshahi and Aude Billard, “A dynamical system approach to task-adaptation in physical human–robot interaction,” *Autonomous Robots*, 43, pp. 927–946, 2019.

[37] Mahdi Khoramshahi and Aude Billard, “A dynamical system approach for detection and reaction to human guidance in physical human–robot interaction,” *Autonomous Robots*, 44, pp. 1411–1429, 2020.

[38] E. C. Townsend, E. A. Mielke, D. Wingate, and M. D. Killpack, “Estimating human intent for physical human-robot co-manipulation,” 2017. https://doi.org/10.48550/arXiv.1705.10851

[39] B. Whitsell and P. Artemiadis, “Physical Human–Robot Interaction (pHRI) in 6 DOF With Asymmetric Cooperation,” in *IEEE Access*, vol. 5, pp. 10834-10845, 2017.

[40] S. S. Ge, Y. Li, and H. He, "Neural-network-based human intention estimation for physical human-robot interaction," *8th International Conference on Ubiquitous Robots and Ambient Intelligence (URAI)*, pp. 390-395, 2011.

[41] Y. Li and S. S. Ge, "Human–Robot Collaboration Based on Motion Intention Estimation," in *IEEE/ASME Transactions on Mechatronics*, vol. 19, no. 3, pp. 1007-1014, 2014.

[42] B. Guler, P. P. Niaz, A. Madani, Y. Aydin, and C. Basdogan, "An adaptive admittance controller for collaborative drilling with a robot based on subtask classification via deep learning," *Mechatronics*, 86:102851, 2022.

[43] W. Lu, Z. Hu, and J. Pan, "Human-Robot Collaboration using Variable Admittance Control and Human Intention Prediction," *IEEE 16th International Conference on Automation Science and Engineering (CASE)*, pp. 1116-1121, 2020.

[44] Kim Tien Ly, Mithun Poozhiyil, Harit Pandya, Gerhard Neumann, and Ayse Kucukyilmaz, "Intent-Aware Predictive Haptic Guidance and its Application to Shared Control Teleoperation," *IEEE International Conference on Robot & Human Interactive Communication (RO-MAN)*, pp. 565-572, 2021.

[45] S. H. Chien, J. H. Wang, and M. Y. Cheng, "Robotic Assistance for Physical Human–Robot Interaction Using a Fuzzy RBF Hand Impedance Compensator and a Neural Network Based Human Motion Intention Estimator," in *IEEE Access*, vol. 9, pp. 126048-126057, 2021.

[46] W. Wang, R. Li, Y. Chen, and Y. Jia. "Human Intention Prediction in Human-Robot Collaborative Tasks," in *Companion of the 2018 ACM/IEEE International Conference on Human-Robot Interaction (HRI '18*), *Association for Computing Machinery*, New York, NY, USA, pp. 279–280, 2018.

[47] D. Sirintuna, I. Ozdamar, Y. Aydin, and C. Basdogan, "Detecting Human Motion Intention during pHRI Using Artificial Neural Networks Trained by EMG Signals," *29th IEEE International Conference on Robot and Human Interactive Communication (RO-MAN)*, pp. 1280-1287, 2020.

[48] C. E. Madan, A. Kucukyilmaz, T. M. Sezgin, and C. Basdogan, "Recognition of haptic interaction patterns in dyadic joint object manipulation," *IEEE Transactions on Haptics*, vol. 8, no. 1, pp. 54–66, 2015.

[49] Z. Al-Saadi, D. Sirintuna, A. Kucukyilmaz, and C. Basdogan, "A Novel Haptic Feature Set for the Classification of Interactive Motor Behaviors in Collaborative Object Transfer," in *IEEE Transactions on Haptics*, vol. 14, no. 2, pp. 384-395, 2021.

[50] A. Kucukyilmaz, and I. Issak, "Online identification of interaction behaviors from haptic data during collaborative object transfer," in *IEEE Robotics and Automation Letters,* vol. 5, no. 1, pp. 96-102, 2020.

[51] Y. Aydin, O. Tokatli, V. Patoglu, and C. Basdogan, "Fractional order admittance control for physical human-robot interaction," in *IEEE World Haptics Conference (WHC),* pp. 257–262, 2017.

[52] Y. Aydin, O. Tokatli, V. Patoglu, and C. Basdogan, "Stable physical human-robot interaction using fractional order admittance control," *IEEE Transactions on Haptics*, vol. 11, no. 3, pp. 464–475, 2018.

[53] Y. Aydin, O. Tokatli, V. Patoglu, and C. Basdogan, "A computational multi-criteria optimization approach to controller design for physical human-robot interaction," *IEEE Transactions on Robotics*, vol. 6, no. 6, pp. 1791-1804, 2020.

[54] S. P. Buerger and N. Hogan, "Complementary stability and loop shaping for improved human–robot interaction," *IEEE Trans. Robot.*, vol. 23, no. 2, pp. 232–244, Apr. 2007.

[55] J. M. Dolan, M. B. Friedman, and M. L. Nagurka, "Dynamic and loaded impedance components in the maintenance of human arm posture," *IEEE Trans. Syst., Man, Cybern.*, vol. 23, no. 3, pp. 698–709, 1993.

[56] T. Tsuji, P. Morasso, K. Goto, and K. Ito, "Human hand impedance characteristics during maintained posture in multi-joint arm movements," *Biol. Cybern.*, vol. 72, pp. 476–485, 1995.

[57] B. Willaert, M. Franken, H. V. Brussel, and E. B. V. Poorten, "On the use of shunt impedances versus bounded environment passivity for teleoperation systems," in *IEEE International Conference on Robotics and Automation*, pp. 2111–2117, 2011.

[58] Y. Aydin, D. Sirintuna, and C. Basdogan, "Towards collaborative drilling with a cobot using admittance controller," *Transactions of the Institute of Measurement and Control*, 43(8), pp. 1760-1773, 2021.

[59] P. M. Fitts, “The information capacity of the human motor system in controlling the amplitude of movement,” *Journal of Experimental Psychology*, vol. 47, no. 6, pp. 381–391, 1954.

[60] R. W. Soukoreff and I. S. MacKenzie, “Towards a standard for pointing device evaluation, perspectives on 27 years of Fitts’ law research in HCI,” *International Journal of Human-Computer Studies*, vol. 61, no. 6, pp. 751–789, 2004.

[61] G. F. Templeton, “A two-step approach for transforming continuous variables to normal: implications and recommendations for IS research,” *Communications of the Association for Information Systems*, vol. 28, pp. 41–58, 2011.

[62] I. S. MacKenzie, “Fitts' law as a research and design tool in human-computer interaction,” *Human Computer Interaction*, vol. 7, pp. 91–139, 1992.

[63] J. Ryu, D. Kwon, and B. Hannaford, “Stability guaranteed control: time domain passivity approach,” *IEEE Transactions on Control Systems Technology*, vol. 12, no. 6, pp. 860–868, 2004.

[64] R. T. O'Brien and P. A. Iglesias, "On the poles and zeros of linear, time-varying systems," in *IEEE Transactions on Circuits and Systems I: Fundamental Theory and Applications*, vol. 48, no. 5, pp. 565-577, May 2001.

[65] K. Liu, “Extension of modal analysis to linear time-varying systems,” *Journal of Sound and Vibration,* 226 (1), pp. 149–167, 1999.

[66] H. Bourlès and B. Marinescu, “Linear Time-Varying Systems,” Springer Berlin Heidelberg, 2011.

[67] O. Khatib, “Real-time obstacle avoidance for manipulators and mobile robots,” in *Proceedings of the IEEE Conference on Robotics and Automation*, pp. 500-505, 1986.

[68] E. Noohi and M. Žefran, “Quantitative measures of cooperation for a dyadic physical interaction task,” in *IEEE-RAS International Conference on Humanoid Robots*, pp. 469–474, 2014.

[69] F. Pedregosa, G. Varoquaux, A. Gramfort, V. Michel, B. Thirion, O. Grisel, M. Blondel, P. Prettenhofer, R. Weiss, V. Dubourg, J. Vanderplas, A. Passos, D. Cournapeau, M. Brucher, M. Perrot, and É. Duchesnay, “Scikit-learn: Machine Learning in Python,” *Journal of Machine Learning Research*, vol. 12, pp. 2825–2830, 2011.

[70] Y. M. Hamad, Y. Aydin, and C. Basdogan, “Adaptive Human Force Scaling via Admittance Control for Physical Human-Robot Interaction,” in *IEEE Transactions on Haptics*, vol. 14, no. 4, pp. 750-761, 2021.

[71] D. Sirintuna, Y. Aydin, O. Caldiran, O. Tokatli, V. Patoglu, and C. Basdogan, “A variable-fractional order admittance controller for pHRI,” *Proceedings of IEEE International Conference on Robotics and Automation (ICRA)*, pp. 10162–10168, 2020.

[72] A. Madani, P. P. Niaz, B. Guler, Y. Aydin, and C. Basdogan, “Robot-Assisted Drilling on Curved Surfaces with Haptic Guidance under Adaptive Admittance Control,” *IEEE/RSJ International Conference on Intelligent Robots and Systems (IROS)*, pp. 3723-3730, 2022.